



1 **Carbon cycle feedbacks in an idealized and a scenario simulation of negative emissions in CMIP6**  
2 **Earth system models**

3

4 Ali Asaadi<sup>1</sup>, Jörg Schwinger<sup>1</sup>, Hanna Lee<sup>1,2</sup>, Jerry Tjiputra<sup>1</sup>, Vivek Arora<sup>3</sup>, Roland Séférian<sup>4</sup>, Spencer  
5 Liddicoat<sup>5</sup>, Tomohiro Hajima<sup>6</sup>, Yera Santana-Falcón<sup>4</sup>, Chris D. Jones<sup>5</sup>

6

7 <sup>1</sup>NORCE Norwegian Research Centre & Bjerknes Centre for Climate Research, Bergen, Norway

8 <sup>2</sup>Department of Biology, Norwegian University of Science and Technology, Trondheim, Norway

9 <sup>3</sup>Canadian Centre for Climate Modelling and Analysis, Environment and Climate Change Canada,  
10 Victoria, BC, Canada

11 <sup>4</sup>CNRM, Université de Toulouse, Météo-France, CNRS, Toulouse, France

12 <sup>5</sup>Met Office Hadley Centre, Exeter, United Kingdom

13 <sup>6</sup>Research Institute for Global Change, Japan Agency for Marine-Earth Science and Technology,  
14 Yokohama 236-0001, Japan

15

16 \*Corresponding author, ali.asaadi@mail.mcgill.ca

17

18 **Abstract**

19 Limiting global warming to 1.5°C by the end of the century is an ambitious target that requires  
20 immediate and unprecedented emission reductions. In the absence of sufficient near term mitigation,  
21 this target will only be achieved by carbon dioxide removal (CDR) from the atmosphere later during this  
22 century, which would entail a period of temperature overshoot. Next to the socio-economic feasibility  
23 of large-scale CDR, which remains unclear, the effect on biogeochemical cycles and climate are key to  
24 assessing CDR as a mitigation option. Changes in atmospheric CO<sub>2</sub> concentration and climate alter the  
25 CO<sub>2</sub> exchange between the atmosphere and the underlying carbon reservoirs of land and the ocean.  
26 Here, we investigate carbon cycle feedbacks under idealized and more realistic overshoot scenarios in  
27 an ensemble of Earth system models. The response of oceanic and terrestrial carbon stocks to changes  
28 in atmospheric CO<sub>2</sub> concentration and changes in surface climate (the carbon-concentration and  
29 carbon-climate feedback, quantified by the feedback metrics  $\beta$  and  $\gamma$ , respectively) show a large  
30 hysteresis. This hysteresis leads to growing absolute values of  $\beta$  and  $\gamma$  during phases of negative  
31 emissions. We find that this growth is spatially quite homogeneous, since the spatial patterns of  
32 feedbacks do not change significantly for individual models. We confirm that the  $\beta$  and  $\gamma$  feedback  
33 metrics are a relatively robust tool to characterize inter-model differences in feedback strength since  
34 the relative feedback strength remains largely stable between phases of positive and negative  
35 emissions and between different simulations, although exceptions exist. When emissions become  
36 negative, we find that the model uncertainty (model disagreement) in  $\beta$  and  $\gamma$  increases stronger than  
37 expected from the assumption that the uncertainties would accumulate linearly with time. This  
38 indicates that the model response to a change from increasing to decreasing forcing introduces an  
39 additional layer of uncertainty, at least in idealized simulations with a strong signal. We also briefly  
40 discuss the existing alternative definition of feedback metrics based on instantaneous carbon fluxes  
41 instead of carbon stocks and provide recommendations for the way forward and future model  
42 intercomparison projects.



## 43 1. Introduction

44 Estimated remaining carbon budgets compatible with limiting anthropogenic warming to 1.5 or 2 °C  
45 above pre-industrial levels are extremely tight and will be exhausted within the next few decades if the  
46 current emission rate is maintained (e.g., Rogelj et al. 2015; Goodwin et al. 2018; V. Masson-Delmotte  
47 et al. 2018). Therefore, unless CO<sub>2</sub> emissions are reduced immediately at an unprecedented rate, the  
48 1.5 or 2°C targets can only be reached after a period of temperature overshoot (Rogelj et al. 2015; Ricke  
49 et al. 2017; Geden and Löschel 2017; Riahi et al. 2021). Although the option to remove large quantities  
50 of carbon from the atmosphere remains speculative (Gasser et al. 2015; Smith et al. 2016; Larkin et al.  
51 2018; Fuss et al. 2018; Creutzig et al. 2019), in such overshoot pathways, too large near-term carbon  
52 emissions would be compensated by large-scale carbon dioxide removal (CDR) later in this century.  
53 Research on negative emissions exploring the reversibility of CO<sub>2</sub>-induced climate change has been  
54 conducted for more than a decade (e.g., Boucher et al. 2012; Wu et al. 2015; Tokarska and Zickfeld  
55 2015; Li et al. 2020; Jeltsch-Thömmes et al. 2020; Yang et al. 2021; Schwinger et al. 2022; Bertini and  
56 Tjiputra 2022). These studies generally report a hysteresis behavior of the Earth system under negative  
57 emission, resulting in greatly varying reversibility for different aspects of the Earth system. While the  
58 surface temperature trend follows a reduction in atmospheric CO<sub>2</sub> relatively closely (e.g., Boucher et  
59 al. 2012; Jeltsch-Thömmes et al. 2020), hysteresis can be large in the interior ocean, making for example  
60 ocean heat content and steric sea level rise as well as interior ocean oxygen content and acidification  
61 largely irreversible on policy relevant timescales (Mathesius et al. 2015; Li et al. 2020; Schwinger et al.  
62 2022; Bertini and Tjiputra 2022). The same is true for the loss of carbon from thawing permafrost soils  
63 (MacDougall et al. 2015; Gasser et al. 2018; Park and Kug 2022; Schwinger et al. 2022).

64 Carbon emissions drive multiple responses of the Earth system via changes in its physical climate and  
65 the biogeochemical carbon cycle. Under increasing atmospheric CO<sub>2</sub> concentrations, increasing carbon  
66 uptake by the ocean and terrestrial biosphere slows down global climate change by removing the  
67 greenhouse gas CO<sub>2</sub> from the atmosphere, a process that is mainly driven by the dissolution of CO<sub>2</sub> into  
68 the oceans (e.g. Revelle and Suess 1957, Siegenthaler and Oeschger 1978) and the CO<sub>2</sub>-fertilisation  
69 effect on the terrestrial biosphere (Schimel et al. 2015). On the other hand, Earth system model (ESM)  
70 simulations show that this carbon uptake is reduced by progressive global warming due to, among  
71 others, changes in ocean circulation and a reduction of CO<sub>2</sub> solubility in warmer waters, as well as  
72 increased respiration rates from soils (Tharammal et al. 2019; Arora et al. 2020; Canadell et al. 2021),  
73 and carbon release from degrading permafrost. These two feedback processes, the response to rising  
74 CO<sub>2</sub> concentrations and the response to climate change, are termed carbon-concentration and carbon-  
75 climate feedback, respectively (Gregory et al. 2009). In the context of overshoot pathways, carbon cycle  
76 feedbacks determine the efficiency of negative emissions as the oceans and the terrestrial biosphere  
77 will first take up carbon at reduced rates and eventually turn into sources of carbon to the atmosphere  
78 (Jones et al. 2016a; Schwinger and Tjiputra 2018).

79 The carbon-concentration and carbon-climate feedbacks can be characterized by feedback metrics, for  
80 example, by feedback factors  $\beta$  and  $\gamma$  (Friedlingstein et al. 2003) that quantify the gain/loss of carbon  
81 in terrestrial or marine reservoirs per unit change in atmospheric CO<sub>2</sub> concentration and temperature,  
82 respectively (see Section 2 for details). These feedback factors are valuable tools to compare the  
83 feedback strength among different models (Friedlingstein et al. 2003, 2006; Yoshikawa et al. 2008; Boer



84 and Arora 2009; Gregory et al. 2009; Roy et al. 2011; Arora et al. 2013, 2020) and can be calculated  
85 using idealized model simulations, in which the effect of CO<sub>2</sub> on the carbon cycle and the radiative effect  
86 of CO<sub>2</sub> are decoupled. In a biogeochemically coupled (BGC) simulation, the radiation code of an ESM  
87 does not respond to increasing atmospheric CO<sub>2</sub> concentrations, but the terrestrial and marine carbon  
88 cycles do. There is little climate change in such a simulation, which can therefore be used to quantify  
89 the carbon-concentration feedback. The difference between a standard (fully coupled, COU) simulation  
90 and the BGC simulation is used to quantify the carbon-climate feedback. In the last two phases of the  
91 Coupled Model Intercomparison Project (CMIP5 and CMIP6, Taylor et al. 2012; Eyring et al. 2016)  
92 carbon cycle feedbacks were addressed by conducting additional decoupled simulations of the standard  
93 1% CO<sub>2</sub> simulation (1pctCO<sub>2</sub> hereafter), which prescribes an increase in atmospheric CO<sub>2</sub> by 1% per  
94 year until quadrupling (Arora et al. 2013, 2020). Next to this idealized simulation, the protocol for the  
95 CMIP6 Coupled Climate-Carbon Cycle Model Intercomparison Project (C4MIP, Jones et al. 2016b) also  
96 proposes a BGC simulation for the SSP5-3.4-OS scenario (O'Neill et al. 2016). This scenario describes an  
97 overshoot pathway, in which emissions increase unmitigated until 2040, but strong mitigation  
98 (including CDR) is undertaken thereafter. In contrast to the 1pctCO<sub>2</sub> simulation, where no forcing other  
99 than atmospheric CO<sub>2</sub> is varied, the quantification of feedbacks in this scenario simulation is  
100 complicated by the presence of land use change and changes in radiative forcing through emissions of  
101 aerosols and non-CO<sub>2</sub> greenhouse gasses (Melnikova et al. 2021, 2022).

102 Permafrost soils in the northern high latitudes have accumulated roughly 1100-1700 Pg of carbon in  
103 the form of frozen organic matter, about twice as much as currently contained in the atmosphere  
104 (Hugelius et al. 2014; Schuur et al. 2015). The release of CO<sub>2</sub> and methane (CH<sub>4</sub>) from thawing  
105 permafrost will amplify global warming due to anthropogenic emissions and further accelerate  
106 permafrost degradation and microbial decomposition (Feng et al. 2020; Smith et al. 2022). This positive  
107 feedback and the fact that Arctic temperatures are increasing twice as fast as the global average  
108 (Jenkins and Dai 2021; Liang et al. 2022) have made permafrost to be considered among the key tipping  
109 elements of the climate system, although it may not be an abrupt but irreversible process (Armstrong  
110 McKay et al. 2022; Yokohata et al. 2020; Lenton et al. 2019). A temporary temperature overshoot might  
111 entail important legacy effects as high latitude ecosystems and the state of permafrost-affected soils  
112 take several centuries to adjust to the new atmospheric condition (de Vrese and Brovkin 2021). Current  
113 generation ESMs are still in their infancy when it comes to representing the complex and often small-  
114 scale processes of permafrost carbon degradation. Here we take advantage of the fact that one of the  
115 CMIP6 ESMs considered in this study has a vertically resolved representation of soil carbon, which  
116 enables us to estimate the contribution of permafrost degradation to the total carbon-climate feedback  
117 for this model.

118 Except for the recent studies by Schwinger and Tjiputra (2018) and Melnikova et al. (2021, 2022) all  
119 previous studies that quantify carbon-concentration and carbon-climate feedbacks are based on ESM  
120 simulations with increasing atmospheric CO<sub>2</sub>. Here, we take advantage of a simulation conducted for  
121 the CMIP6 Carbon Dioxide Removal Model Intercomparison Project (CDRMIP, Keller et al. 2018) that  
122 mirrors the 1pctCO<sub>2</sub> simulation by prescribing a decrease of atmospheric CO<sub>2</sub> by 1% per year (1pctCO<sub>2</sub>-  
123 cdr). We complement this simulation with a BGC simulation (1pctCO<sub>2</sub>-cdr-bgc) to quantify, in a manner  
124 consistent with previous feedback studies (Arora et al. 2013, 2020), carbon-concentration and carbon-



125 climate feedbacks under negative emissions in an ensemble of CMIP6 ESMs. We complement these  
126 previous studies by a spatial analysis of feedback patterns, and compare the feedbacks from the  
127 positive and negative emission phases of the 1pctCO<sub>2</sub> and 1pctCO<sub>2</sub>-cdr simulations to the feedbacks  
128 obtained from the SSP5-3.4-OS scenario. For the latter, land use change has been shown to have a  
129 dominant effect over carbon-concentration or carbon-climate feedbacks by Melnikova et al. (2021,  
130 2022), and these authors present a more detailed analysis of the role of land use change in the SSP5-  
131 3.4-OS scenario. Since land use change is not a feedback process, we focus in this study on regions that  
132 are not dominated by agricultural areas when comparing feedbacks between the SSP5-3.4-OS and  
133 1pctCO<sub>2</sub> simulations.

134 The purpose of this study is to investigate the evolution of carbon cycle feedbacks and their uncertainty  
135 under deployment of negative emissions. Since feedback metrics are known to depend on the emission  
136 (or concentration) pathway, we investigate the relative feedback strength and the spatial patterns of  
137 feedbacks between positive and negative emission phases as well as between idealized and scenario  
138 simulations. We also briefly explore the contribution of permafrost carbon losses to the carbon-climate  
139 feedback and the impact of alternative feedback metric definitions in the context of negative emissions.

140

## 141 **2. Description of feedback metrics, simulations, and models**

### 142 **2.1 Carbon cycle feedback metrics**

143 The sensitivity of the carbon cycle to changes in atmospheric CO<sub>2</sub> concentration ([CO<sub>2</sub>]) and its  
144 sensitivity to changes in physical climate can be measured using two feedback metrics, which can be  
145 based on either changes in carbon stocks (as introduced by Friedlingstein et al., 2003) or instantaneous  
146 carbon fluxes (as introduced by Boer and Arora 2009). Changes in carbon stocks are equivalent to the  
147 time-integrated carbon fluxes across the air-land and air-sea interfaces, such that for the Friedlingstein  
148 et al. approach (referred to as integrated flux-based approach), the two feedback metrics are:

- 149 1.  $\beta$  (PgC/ppm), which quantifies the strength of the carbon-concentration feedback, i.e., the  
150 changes in oceanic and terrestrial carbon stocks ( $\Delta C_{L,O}$ ) in response to changes in atmospheric  
151 CO<sub>2</sub> concentration ( $\Delta[CO_2]$ ), and
- 152 2.  $\gamma$  (PgC/°C), which measures the strength of the carbon-climate feedback, i.e., changes in land  
153 and ocean carbon stocks ( $\Delta C_{L,O}$ ) in response to changes in global average surface temperature  
154 ( $\Delta T$ ), where  $\Delta T$  serves as a proxy for climate change.

155 Carbon feedback analysis requires, in addition to a standard fully coupled (COU) simulation, a  
156 biogeochemically (BGC) coupled simulation. In a BGC simulation, atmospheric [CO<sub>2</sub>] is kept constant at  
157 its pre-industrial values for the radiative transfer calculations, to isolate the response of land and ocean  
158 biogeochemistry to rising [CO<sub>2</sub>] in the absence of CO<sub>2</sub>-induced climate change. Using this pair of  
159 simulations (COU and BGC) results in the following expressions for  $\beta$  and  $\gamma$  (see Schwinger et al. 2014  
160 for a derivation).



$$\beta_X = \frac{1}{\Delta[CO_2]} \left( \frac{\Delta C_X^{BGC} \Delta T^{COU} - \Delta C_X^{COU} \Delta T^{BGC}}{\Delta T^{COU} - \Delta T^{BGC}} \right) \approx \frac{\Delta C_X^{BGC}}{\Delta[CO_2]} \quad (1)$$

$$\gamma_X = \frac{\Delta C_X^{COU} - \Delta C_X^{BGC}}{\Delta T^{COU} - \Delta T^{BGC}} \approx \frac{\Delta C_X^{COU} - \Delta C_X^{BGC}}{\Delta T^{COU}} \quad (2)$$

where  $X$  can be either  $L$  for land or  $O$  for ocean. Although there is no change in the radiative forcing of  $CO_2$  in the BGC simulation (such that we could expect  $\Delta T^{BGC} = 0$ ), surface temperature can vary due to changes in other radiative forcing agents (aerosols and non- $CO_2$  greenhouse gasses). Even in the idealized 1pct $CO_2$  simulation, where  $CO_2$  is the only variable forcing, there are some climatic changes over the land surface due to a reduction in latent heat fluxes associated with stomatal closure at higher  $CO_2$  levels, as well as changes in vegetation structure, coverage, and composition (Arora et al. 2020), which result in a small temperature increase along with changes in precipitation and soil moisture. The assumption of  $\Delta T^{BGC} = 0$  will simplify equations (1) and (2) such that the rightmost term holds. The instantaneous flux-based approach is equivalent to equations (1) to (2) except that the deviation of the carbon pools  $\Delta C_X$  are replaced by the instantaneous air-sea or air-land carbon fluxes  $F_X$ . To distinguish these feedback metrics from the integrated flux-based ones, the capital letters  $B$  and  $\Gamma$  are used to denote them. The units of  $B$  and  $\Gamma$  are  $PgCyr^{-1}ppm^{-1}$  and  $PgCyr^{-1}C^{-1}$ , respectively.

It is worth mentioning that these idealized feedback frameworks should be seen as a technique for assessing the relative sensitivities of models and understanding their differences (i.e. the model uncertainty of the estimated feedbacks), rather than as absolute measures of invariant system properties (Gregory et al. 2009; Ciais et al. 2013). Therefore, the values of carbon cycle feedback metrics can vary over time within a model simulation (e.g. Arora et al. 2013) or between different scenarios (Hajima et al. 2014).

To gain insight into the reasons for differing responses among models, we apply the decomposition of the simplified expression for  $\beta_L$  (Eq. 1, assuming  $\Delta T^{BGC} = 0$ ) following Arora et al. (2020). This allows us to investigate the contributions from different processes to changes in vegetation and soil carbon reservoirs ( $\Delta C_V$  and  $\Delta C_S$ , respectively).

$$\beta_L = \frac{\Delta C_L^{BGC}}{[CO_2]} = \frac{\Delta C_V^{BGC} + \Delta C_S^{BGC}}{[CO_2]} = \left( \frac{\Delta C_V^{BGC}}{\Delta NPP^{BGC}} \frac{\Delta NPP^{BGC}}{\Delta GPP^{BGC}} \frac{\Delta GPP^{BGC}}{[CO_2]} \right) + \left( \frac{\Delta C_S^{BGC}}{\Delta R_h^{BGC}} \frac{\Delta R_h^{BGC}}{\Delta LF^{BGC}} \frac{\Delta LF^{BGC}}{[CO_2]} \right) = \tau_{cveg\Delta} CUE_{\Delta} \frac{\Delta GPP^{BGC}}{[CO_2]} + \tau_{csoil\Delta} \frac{\Delta R_h^{BGC}}{\Delta LF^{BGC}} \frac{\Delta LF^{BGC}}{[CO_2]} \quad (3)$$

$\Delta NPP$ ,  $\Delta GPP$ ,  $\Delta R_h$ , and  $\Delta LF$  represent deviations of the net primary productivity, gross primary productivity, heterotrophic respiration, and litterfall flux, respectively, from their pre-industrial values. The terms  $\tau_{cveg\Delta}$  and  $\tau_{csoil\Delta}$  are turnover times (in years) of carbon in the vegetation and litter plus



195 soil pools.  $\frac{\Delta NPP}{\Delta GPP}$  is a measure of carbon use efficiency for the fraction of GPP (above its pre-industrial  
196 value) that turned into NPP after subtracting autotrophic respiration losses (denoted as  $CUE_{\Delta}$ ).  
197  $\frac{\Delta GPP}{[CO_2]}$  ( $\text{PgCyr}^{-1}\text{ppm}^{-1}$ ) and  $\frac{\Delta R_h}{\Delta LF}$  are a measure of the global  $CO_2$  fertilization effect and the increase in  
198 heterotrophic respiration per unit increase in litterfall rate, respectively. Also,  $\frac{\Delta LF}{[CO_2]}$  ( $\text{PgCyr}^{-1}\text{ppm}^{-1}$ )  
199 measures the global increase in litterfall rate per unit increase in  $CO_2$ .

200  
201

## 202 **2.2 Model simulations**

203 The 1pctCO2 experiment is a highly idealized model experiment that prescribes a rate of 1% per year  
204 increase in  $[CO_2]$  from pre-industrial values until quadrupling after 140 years. No other forcings are  
205 varied in this experiment, i.e., land use as well as non- $CO_2$  greenhouse gasses and aerosol  
206 concentrations are held constant at their pre-industrial levels. This experiment has already been  
207 performed by the first coupled atmosphere-ocean general circulation models in the late 1980s, and  
208 important climate metrics such as the transient climate response (TCR; Meehl et al. 2020) and the  
209 transient response to cumulative emissions (TCRE; e.g. Gillett et al. 2013) are formally defined through  
210 the 1pctCO2 simulation. Likewise, the C4MIP carbon cycle feedback analysis for the last two phases of  
211 CMIP (Arora et al. 2013, 2020) relied on this simulation. Given the importance of the 1pctCO2  
212 experiment, the CMIP6 CDRMIP protocol proposes an experiment that mirrors the 1pctCO2 simulation  
213 by starting from its endpoint at year 140 and decreasing atmospheric  $CO_2$  at a rate of 1% per year until  
214 pre-industrial  $[CO_2]$  is restored (1pctCO2-cdr). This experiment is designed to investigate the response  
215 of the Earth system to carbon dioxide removal in an idealized fashion. We note that the implied rates  
216 of CDR in the 1pctCO2-cdr simulation are huge and not practically feasible. Also, there is a jump from  
217 very large positive to very large negative diagnosed emissions at the end of year 140, which is clearly  
218 unrealistic. To investigate carbon cycle feedbacks under CDR, we have complemented the 1pctCO2-cdr  
219 simulation with a biogeochemical coupled 1pctCO2-cdr-bgc simulation that starts from the endpoint of  
220 the 1pctCO2-bgc simulation at year 140.

221 The family of Shared Socioeconomic Pathways (SSPs, O'Neill et al. 2014) is designed to represent  
222 different socio-economic futures that social, demographic, political, and economic developments could  
223 lead to. These narrative SSPs are the basis for a set of quantitative future scenarios, a selection of which  
224 is now being used as input for scenario simulations by the latest ESMs in the frame of the CMIP6  
225 ScenarioMIP (O'Neill et al. 2016). The SSP5-3.4-OS scenario follows the high emission SSP5-8.5 pathway  
226 until 2040 at which point strong mitigation policies are introduced to rapidly reduce emissions to zero  
227 by about 2070 and to net-negative levels thereafter (Fig. 3 of O'Neill et al. 2016). In contrast to the  
228 1pctCO2 simulation, the SSP5-3.4-OS scenario includes land use change as well as time varying forcing  
229 from aerosols and non- $CO_2$  greenhouse gasses throughout the simulation period (Fig. 1 of Liddicoat et  
230 al. 2021). For this study, we use the 1pctCO2, 1pctCO2-cdr, and SSP5-3.4-OS simulations from the  
231 CMIP6 archive together with the corresponding biogeochemically coupled simulations of these  
232 experiments. We note that the biogeochemically coupled 1pctCO2-cdr-bgc experiment is not part of  
233 CMIP6, but has been performed for this study by participating modelling groups.



234 The C4MIP simulation protocol does not allow to separate carbon release (or uptake) through land use  
 235 changes from the carbon-concentration feedback, since land use is active in the biogeochemically  
 236 coupled SSP5-3.4-OS simulation. To focus on carbon cycle feedbacks, we eliminate the effect of land  
 237 use changes as much as possible by identifying regions that are mostly unaffected by human activity  
 238 (referred to as “natural land”). To accomplish this in a way that available CMIP6 output permits, we  
 239 define natural land as grid cells with a maximum (over the period 2015 to 2100) crop-land fraction of  
 240 less than 25%. The threshold of 25% used here for our heuristic approach, is a compromise between  
 241 accuracy (some signal of land use change is still present) and spatial coverage (with increasingly lower  
 242 thresholds, larger areas of the globe are excluded). Our results are not very sensitive to variations in  
 243 the threshold between approximately 10 and 30%. Maps of maximum SSP5-3.4-OS cropland fraction  
 244 for each model (Fig. S1) indicates that a 25% threshold reasonably identifies hotspots of agricultural  
 245 production. To make our analysis comparable between the SSP5-3.4-OS and 1pctCO2 simulations, we  
 246 use the same set of grid cells also for the 1pctCO2 simulation (unless otherwise noted), even though  
 247 land cover is not changed from its pre-industrial state in this simulation.  
 248

### 249 2.3 Participating Earth System Models

250 Table 1 summarizes the five ESMs that contributed to this study along with the experiments used for  
 251 the analyses presented here. The primary features of these models are listed in Table 2 of Arora et al.  
 252 (2020). MIROC-ES2L, NorESM2-LM (which employs version 5 of the Community Land Model, CLM5),  
 253 and UKESM1-0-LL have a representation of the terrestrial nitrogen cycle implemented and coupled to  
 254 their carbon cycle. Only the UKESM1-0-LL model has a land component that dynamically simulates  
 255 vegetation cover and competition between their plant functional types (PFTs). Fire is included in the  
 256 CNRM-ESM2-1 and NorESM2-LM models. NorESM2-LM, is the only ESM with vertically resolved soil  
 257 carbon, which allows studying the impact of warming on the carbon stored in permafrost soils in more  
 258 detail. In this study, the gridcell was considered permafrost where the pre-industrial maximum active  
 259 layer thickness was shallower than three meters.

260

261 **Table 1:** List of CMIP6 ESMs used in this study, names of their biogeochemical component models, resolution  
 262 and experiment variants used.

	CanESM5	CNRM-ESM2-1	MIROC-ES2L	NorESM2-LM	UKESM1-0-LL
<b>Atmosphere and land resolution</b>	2.81°x2.81°*	1.4°x1.4°	2.81°x2.81°	1.9°x2.5°	1.875°x1.25°
<b>variant</b>	r1i1p1f1 & r1i1p2f1*	r1i1p1f2	r1i1p1f2	r1i1p1f1	r4i1p1f2 & r1i1p1f2
<b>Ocean resolution</b>	1° (finer in the tropics)	1° (finer in the tropics)	1° (finer close to North Pole and Equator)	1° (finer near the Equator)	1°
<b>Ocean model name</b>	CMOC (biology); carbonate	PISCESv2-gas	OECO2	iHAMOCC	MEDUSA-2.1



	chemistry follows OMIP protocol				
<b>Land model name</b>	CLASS-CTEM	ISBA-CTRIP	MATSIRO (physics), VISIT-e (BGC)	CLM5	JULES-ES-1.0
<b>Reference</b>	Swart et al. (2019)	Séférian et al. (2019)	Hajima et al. (2020)	Tjiputra et al. (2020); Seland et al. (2020)	Sellar et al. (2019)

263 \*CMIP6 experiment variant used across different simulations including: piControl, historical, hist-bgc, ssp585, ssp585-bgc,  
 264 ssp534-over, ssp534-over-bgc, 1pctCO2, 1pctCO2-bgc, 1pctCO2-cdr, and 1pctCO2-cdr-bgc experiments.

265

### 266 3. Results and Discussion

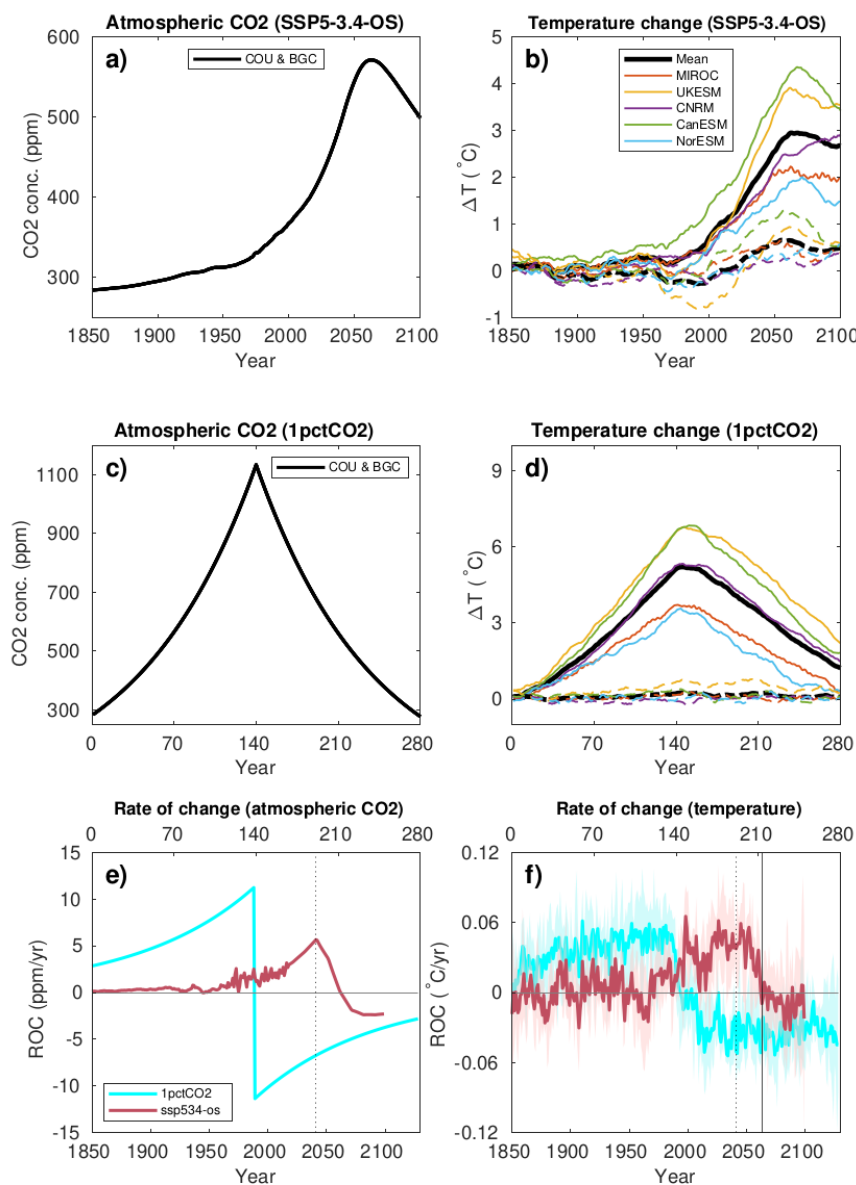
#### 267 3.1 Atmospheric CO<sub>2</sub>, temperature, and carbon fluxes

268 The atmospheric CO<sub>2</sub> concentration ([CO<sub>2</sub>]) for the concentration-driven SSP5-3.4-OS scenario, peaks  
 269 at 571 ppm (a doubling of pre-industrial CO<sub>2</sub> concentration) in the year 2062 and decreases to 497 ppm  
 270 in 2100 (Fig. 1a). According to the scenario design (see O'Neill et al. 2016), strong mitigation policies  
 271 (including deployment of bioenergy with carbon capture and storage (BECCS) and other carbon dioxide  
 272 removal technologies) start in 2040 resulting in an immediate decrease in the CO<sub>2</sub> growth rate that  
 273 peaks in 2041 (Fig. 1e). In the 1pctCO<sub>2</sub> simulation, the prescribed [CO<sub>2</sub>] is symmetric around its 4xCO<sub>2</sub>  
 274 peak of 1133 ppm in the year 140 (Fig. 1c). The rate of change of the CO<sub>2</sub> concentration (Fig. 1e) is very  
 275 different between SSP5-3.4-OS and 1pctCO<sub>2</sub> experiments. In particular, the CO<sub>2</sub> growth rate in the  
 276 idealized 1pctCO<sub>2</sub> experiment has a sudden and large jump from positive to negative values at the  
 277 transition from the ramp-up to the ramp-down phase.

278 The five participating ESMs show large differences in global mean surface air temperature change,  
 279 relative to pre-industrial values, under the SSP5-3.4-OS simulation (Fig. 1b). Peak temperatures vary  
 280 from 2°C in NorESM2-LM to 4.35°C in CanESM5. The timing of the global surface air temperature peak  
 281 varies from 2062 for the MIROC-ES2L and UKESM1-0-LL models to 2100 for CNRM-ESM2-1. After this  
 282 peak, the temperature declines again (except for CNRM-ESM2-1) reaching end-of-the-century values  
 283 that range from 1.39°C above pre-industrial in NorESM2-LM to 3.47°C in CanESM5. The multi-model  
 284 mean global surface air temperature is 2.66°C at the end of the 21st century. The model-mean growth  
 285 rate of the global surface air temperature (Fig. 1f) plateaus at about 0.05°C/yr between approximately  
 286 2030-2050 before it starts to decline to below zero towards the end of the simulation.

287 Temperature changes in the BGC simulation of SSP5-3.4-OS are not negligible since the non-CO<sub>2</sub> forcing  
 288 agents as well as land use change do evolve in time in this scenario, in contrast to the idealized 1pctCO<sub>2</sub>  
 289 simulation. Positive peak temperature anomalies range from 0.37°C (CNRM-ESM2-1 in 2098) to 1.29°C  
 290 (CanESM5 in 2057). UKESM1-0-LL also shows a pronounced negative temperature anomaly during the  
 291 historical period of the BGC simulation of -0.80°C in the year 1990.





292

293

294

295

296

297

298

299

300

**Figure 1:** Atmospheric CO<sub>2</sub> concentration and surface air temperature changes in the fully coupled (solid lines) and biogeochemically coupled (dashed lines) configurations of the SSP5-3.4-OS (a,b) and 1pctCO<sub>2</sub> (c,d) experiments. The rates of change in the prescribed atmospheric CO<sub>2</sub> concentrations is shown in panel e, and the model mean rate of surface temperature change from the fully coupled simulations is shown in panel f. The dotted (solid) vertical lines in panels e and f indicate the peak of the CO<sub>2</sub> growth rate (CO<sub>2</sub> concentration) in the SSP5-3.4-OS scenario. Shadings in panel f show the range across the models. An 11-year moving average has been used in panels b, d, and f.

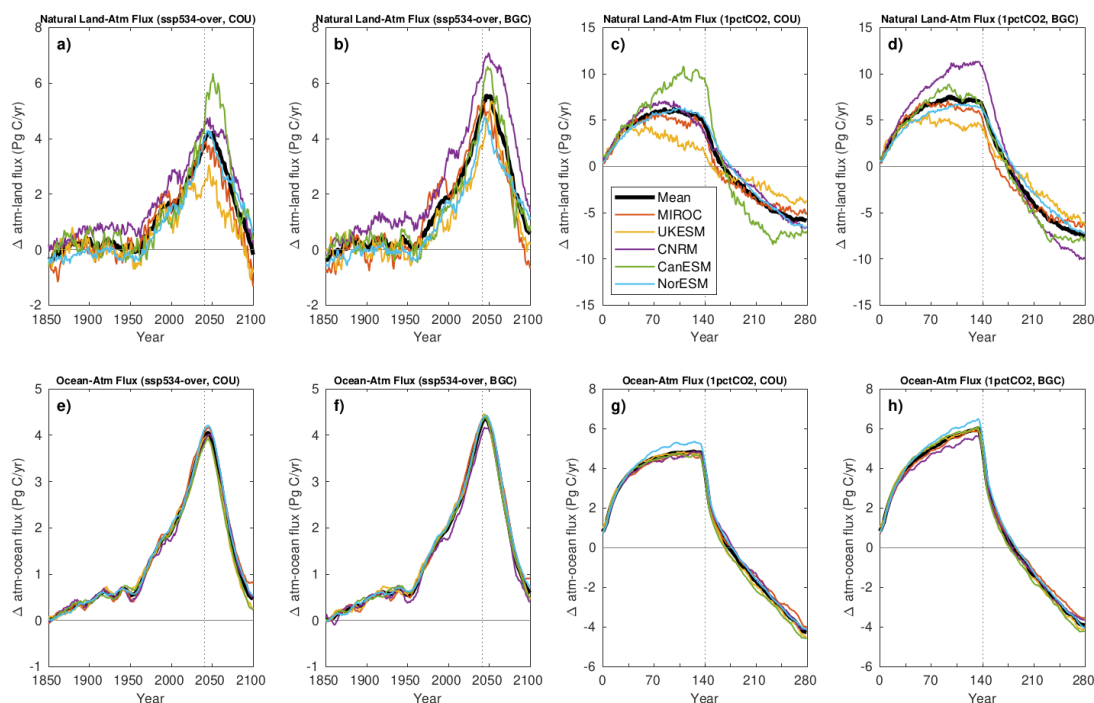


301 In the 1pctCO<sub>2</sub> simulation, the peak temperature anomalies vary from 3.57°C (in year 144) in NorESM2-  
302 LM to 6.84°C (in year 151) in CanESM5 (Fig. 1d). Thereafter, temperature anomalies decline to values  
303 ranging from 0.29°C in NorESM2-LM to 2.2°C in UKESM1-0-LL at the end of the ramp-down period (year  
304 280). The 1pctCO<sub>2</sub> BGC simulation shows, compared to the SSP5-3.4-OS BGC simulation, smaller  
305 temperature anomalies ranging from -0.22°C (CNRM-ESM2-1 in year 149) to 0.79°C (UKESM1-0-LL in  
306 year 207). The smaller magnitude of the temperature anomaly in the BGC simulation of the SSP5-3.4-  
307 OS scenario compared to the 1pctCO<sub>2</sub>-BGC simulations (also given the much higher CO<sub>2</sub> forcing in the  
308 latter) suggests that a substantial part of the carbon-climate feedback in the SSP5-3.4-OS scenario might  
309 be caused by non-CO<sub>2</sub> forcings.

310 For atmosphere-land fluxes, our analysis is complicated by the fact that land use changes are present  
311 in the SSP5-3.4-OS scenario. Here, we focus on comparing fluxes and feedbacks for grid cells that are  
312 dominated by “natural land” (see Sec. 2.2 for more details). Note that, for comparability, we consider  
313 the same set of grid cells in the 1pctCO<sub>2</sub> simulation, even though land cover stays at its pre-industrial  
314 state in this simulation. In the SSP5-3.4-OS simulations, the model-mean annual CO<sub>2</sub> fluxes (Fig. 2)  
315 continue rising until the rate of change of [CO<sub>2</sub>] reaches its peak in 2041. After the peak, natural  
316 atmosphere-land and atmosphere-ocean fluxes start to decline rapidly in all models with little time lag.  
317 UKESM1-0-LL and MIROC-ES2L simulate negative fluxes (i.e., natural land turns into a carbon source)  
318 before the end of the 21st century in the COU simulation (Fig. 2a). Without the effect of CO<sub>2</sub> induced  
319 warming (BGC simulation, Fig. 2b), only MIROC-ES2L shows a significant carbon source from the  
320 terrestrial biosphere before 2100, while the model-mean still shows a sink. In the fully coupled 1pctCO<sub>2</sub>  
321 experiment, sink-to-source transition of the terrestrial biosphere occurs around year 165 in the model  
322 mean, 25 years after the rate of change of [CO<sub>2</sub>] peaks (Fig. 2c). Consistent with what is seen in the  
323 biogeochemically coupled SSP5-3.4-OS, the sink-to-source transition occurs 10 years later without the  
324 effect of warming in the 1pctCO<sub>2</sub>-BGC experiment. However, the terrestrial CO<sub>2</sub> source at the end of  
325 the biogeochemically coupled 1pctCO<sub>2</sub> simulation is *larger* than in the fully coupled simulation. We also  
326 observe (Fig. 2c,d) that models which take up more (less) terrestrial carbon during the CO<sub>2</sub> ramp-up  
327 phase (1pctCO<sub>2</sub>) release more (less) carbon towards the end of the CO<sub>2</sub> ramp-down phase (1pctCO<sub>2</sub>-  
328 cdr-bgc). We therefore interpret the increased source of carbon at the end of the 1pctCO<sub>2</sub>-BGC  
329 simulation as an outgassing of the excess carbon that could be taken up in the absence of climate  
330 warming. The net negative emission phase of the SSP5-3.4-OS scenario is too short to show this effect  
331 in 2100 (where the warming effect still *increases* the terrestrial carbon source).

332 Likewise, the warming of the world's oceans in both simulations, tends to reduce the carbon uptake or  
333 increase the oceanic carbon source. The model spread for atmosphere-ocean carbon fluxes (Fig. 2,  
334 panels e to h) appears to be much smaller than for the atmosphere-land fluxes. In the SSP5-3.4-OS  
335 simulation, the ocean remains a sink of carbon in all models until the end of the simulation in 2100. In  
336 the 1pctCO<sub>2</sub> simulation the ocean turns into a source of CO<sub>2</sub> to the atmosphere around year 175, and  
337 in the BGC simulation without warming this transition is delayed by 7 years.

338



339

340

341

342

343

344

345

346

**Figure 2:** Time series of annual mean natural atmosphere-land (a-d) and atmosphere-ocean (e-h) carbon fluxes for the fully and biogeochemically coupled SSP5-3.4-OS and 1pctCO<sub>2</sub> experiments as indicated in the panel titles. The dotted vertical lines indicate where [CO<sub>2</sub>] growth rate peaks in each experiment. An 11-year moving average has been used in all panels.

347

348

349

350

351

352

353

354

355

356

357

### 3.2 Global mean carbon cycle feedbacks

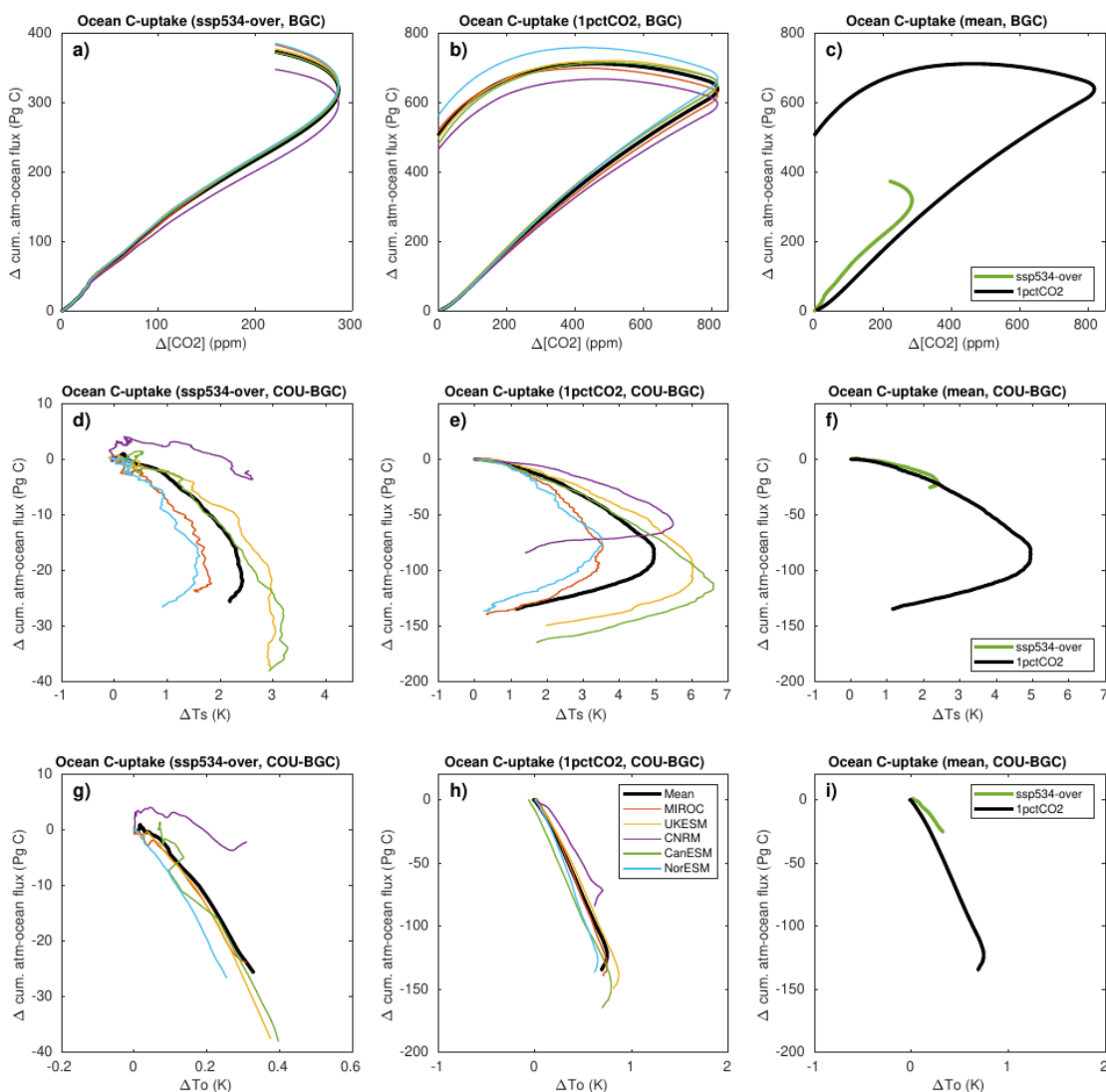
#### 3.2.1 Ocean

In the BGC simulation, where the effect of changing atmospheric CO<sub>2</sub> concentration on terrestrial and marine carbon uptake (the carbon-concentration feedback) is isolated, cumulative atmosphere-ocean carbon fluxes indicate an almost linear growth with [CO<sub>2</sub>] as long as atmospheric CO<sub>2</sub> concentrations are increasing in both SSP5-3.4-OS and 1pctCO<sub>2</sub> simulations (Fig. 3a-c). When [CO<sub>2</sub>] starts to decline, the atmosphere-ocean carbon flux in the 1pctCO<sub>2</sub> simulation shows pronounced hysteresis with a continued ocean carbon uptake (until the [CO<sub>2</sub>]-anomaly has been roughly reduced to 500 ppm) before starting to decrease towards the end of the ramp-down phase (Fig. 3b). In the SSP5-3.4-OS BGC scenario, where the onset of net negative emissions is more gradual, the relationship between cumulative atmosphere-ocean fluxes and [CO<sub>2</sub>] during the phase of declining atmospheric CO<sub>2</sub> concentration also shows hysteresis; but due to the relative short period of net-negative emissions, the ocean remains a sink of carbon in all models until the end of the simulation.



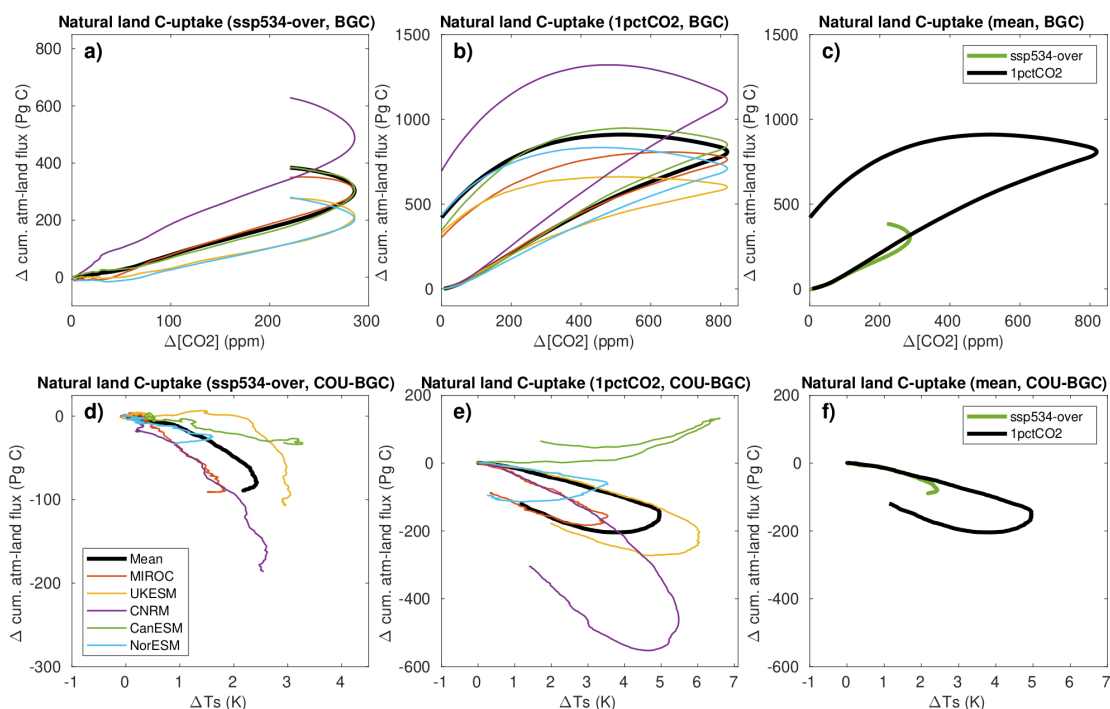
358 Differences in the cumulative atmosphere-ocean CO<sub>2</sub> flux between the COU and the BGC simulations  
359 versus surface temperature changes (carbon-climate feedback) are shown in Fig. 3d-f. Increasing  
360 temperature results in less carbon uptake by the ocean, except for the CNRM-ESM2-1 which simulates  
361 slightly more uptake in the first half of the warming period under the SSP5-3.4-OS. During the negative  
362 emission phases of the simulations when the air surface temperature is decreasing, the carbon-climate  
363 feedback still decreases the ocean carbon content, albeit at reduced rates. Even when pre-industrial  
364 CO<sub>2</sub> concentrations are restored at the end of the 1pctCO<sub>2</sub> simulation all models agree that the ocean  
365 is still losing carbon due to the effect of (legacy) warming (Fig. 3e). Using the global average ocean  
366 potential temperature (averaged over the full ocean depth) instead of the surface air temperature as a  
367 proxy for oceanic climate change as proposed by Schwinger and Tjiputra (2018), gives a much more  
368 linear relationship between changes in the ocean carbon stock and changes in temperature in the  
369 majority of models (Fig. 3 g-i). At the end of the simulations, the ocean still holds a large part of the  
370 carbon taken up from the atmosphere since pre-industrial time, between roughly 300-400 PgC in  
371 1pctCO<sub>2</sub>, and around 350 PgC in SSP5-3.4-OS (Fig. S2).

372 Generally, the ocean carbon-concentration feedback is larger in the SSP5-3.4-OS scenario, which can  
373 most likely be explained with the slower growth rate of [CO<sub>2</sub>] in this scenario compared to the 1pctCO<sub>2</sub>  
374 simulation (Fig. 3c). For slower growth rates, the ocean has more time to mix and partly transport the  
375 adsorbed anthropogenic carbon away from the ocean surface to the interior, increasing the capacity  
376 for more uptake. A larger carbon uptake at slower CO<sub>2</sub> growth rates has already been reported by  
377 Gregory et al. 2009 and Hajima et al. 2014, although only for combined land and ocean fluxes or land  
378 fluxes only. The ocean carbon-climate feedback, in contrast, is slightly smaller in the SSP5-3.4-OS  
379 scenario, i.e., the carbon loss for a given warming is smaller.



380  
 381 **Figure 3:** Ocean carbon cycle feedbacks in the SSP5-3.4-OS (left column) and 1pctCO<sub>2</sub> (middle column)  
 382 simulations for individual models. The model means for both simulations are shown in the right column.  
 383 Global mean ocean potential temperature is used on the x-axis of panels (g-i). An 11-year moving  
 384 average has been used in all panels.

385  
 386  
 387  
 388  
 389



390

391

392 **Figure 4:** Terrestrial carbon cycle feedbacks in the SSP5-3.4-OS (left column) and 1pctCO2 (middle

393 column) simulations for grid cells that are dominated by “natural land” (less than a maximum of 25%

394 crop fraction over the period 2015-2100 in SSP5-3.4-OS). Note that we consider the same grid cells in

395 the 1pctCO2 simulation, even though land use stays at pre-industrial state. The model means for both

simulations are shown in the right column. An 11-year moving average has been used in all panels.

396

### 397 3.2.2 Land

398 For grid cells representing natural land, the response of the cumulative terrestrial carbon flux to

399 changes in [CO<sub>2</sub>] and surface temperature (Fig. 4) is qualitatively similar to the response of the

400 atmosphere-ocean fluxes. In both SSP5-3.4-OS and 1pctCO2 simulations, a roughly linear relationship

401 can be seen between the carbon flux change and both the changes in [CO<sub>2</sub>] and surface air temperature

402 during positive emission phases. An exception is the carbon-climate feedback of the CanESM5 model,

403 which is about zero up to 4 degrees of warming, and becomes positive for higher temperature

404 increases. This unique behavior is caused by CanESM5’s high climate sensitivity combined with larger

405 carbon use efficiency amongst CMIP6 models (as shown later) which causes high latitude vegetation to

406 take up large amounts of carbon in response to warming. This more than compensates for the carbon

407 loss elsewhere associated with climate warming. During negative emission phases both feedbacks show

408 a considerable hysteresis behavior, as for the ocean (see also below).

409 The carbon-concentration feedback is slightly smaller for the SSP5-3.4-OS scenario compared to the

410 1pctCO2 experiment (see Fig. 4c), but this difference might be attributed to the remaining influence of

411 land-use changes. This is because, for “crop-land grid cells” (maximum crop-fraction of more than 25%



412 in the SSP5-3.4-OS scenario), the cumulative carbon fluxes are markedly smaller in the SSP5-3.4-OS  
413 scenario compared to the 1pctCO<sub>2</sub> simulation (compare panel c on Figs. S3 and 4). This indicates,  
414 consistent with the results of Melnikova et al. (2022), that the prescribed land use change in the SSP  
415 scenario is the driver behind the small (negative for NorESM2-LM and UKESM) carbon accumulation for  
416 crop land grid cells. We note that land use change is not a feedback process, and it obviously does not  
417 depend on atmospheric CO<sub>2</sub> concentration. It is only due to the simulation design used here (see Section  
418 2.2 for details), that the carbon release (or uptake) due to land use changes modifies the net  
419 atmosphere-land CO<sub>2</sub> flux which is then seen as a carbon-concentration feedback in the SSP5-3.4-OS-  
420 BGC simulation.

421 The model-mean carbon-climate feedback for natural land is very similar for the SSP5-3.4-OS and  
422 1pctCO<sub>2</sub> simulations during the positive emission phases, but deviates thereafter due to hysteresis  
423 behavior (Fig. 4f). Interestingly, in contrast to the carbon-concentration feedback, the global average  
424 carbon-climate feedback for cropland and natural land remains very similar between the SSP5-3.4-OS  
425 and 1pctCO<sub>2</sub> simulations (Fig. S3). This is likely due to the similar response of the soil carbon to changes  
426 in surface air temperature.

427

### 428 3.2.3 Hysteresis

429 For the 1pctCO<sub>2</sub> simulation, hysteresis can be defined as the difference in, for example, cumulative  
430 carbon uptake during the ramp-up and the ramp-down period at the same level of atmospheric CO<sub>2</sub>  
431 concentration. Here, to quantify hysteresis, we choose the years 70 and 210, which represent a state  
432 where atmospheric CO<sub>2</sub> has been doubled (570 ppm) or returned to this value after the overshoot. We  
433 refrain from quantifying hysteresis for the SSP5-3.4-OS scenario, because of the relatively short period  
434 of declining [CO<sub>2</sub>].

435 The model mean hysteresis in the carbon-concentration feedback is  $443 \pm 29$  PgC (model uncertainty  
436 measured as one standard deviation) for the ocean and  $524 \pm 205$  PgC for natural land, which for both  
437 cases is larger than the feedback at year 70 itself. Although the hysteresis of the ocean carbon-  
438 concentration feedback is smaller than the terrestrial feedback in absolute terms, it is larger in relative  
439 terms (179% of the accumulated carbon uptake at year 70 for the ocean versus 168% for land). In  
440 general, the hysteresis seems to be related to the magnitude of the carbon-concentration feedback,  
441 since models with a large (small) carbon uptake at year 140, tend to show a large (small) hysteresis at  
442 year 210 for both ocean and land. However, towards the end of the ramp-down period, this relationship  
443 breaks down for CanESM5 and MIROC, particularly over land.

444 For the carbon-climate feedback, the hysteresis in climate induced carbon loss or gain (difference  
445 between COU-BGC evaluated at years 70 and 210) is  $-102 \pm 22$  and  $-158 \pm 181$  PgC for ocean and natural  
446 land, respectively. As for the carbon-concentration effect, a relationship between the magnitude of  
447 carbon loss or gain at year 140 and the hysteresis is found. Models with a large (small) climate induced  
448 loss of carbon tend to have a large (small) hysteresis.



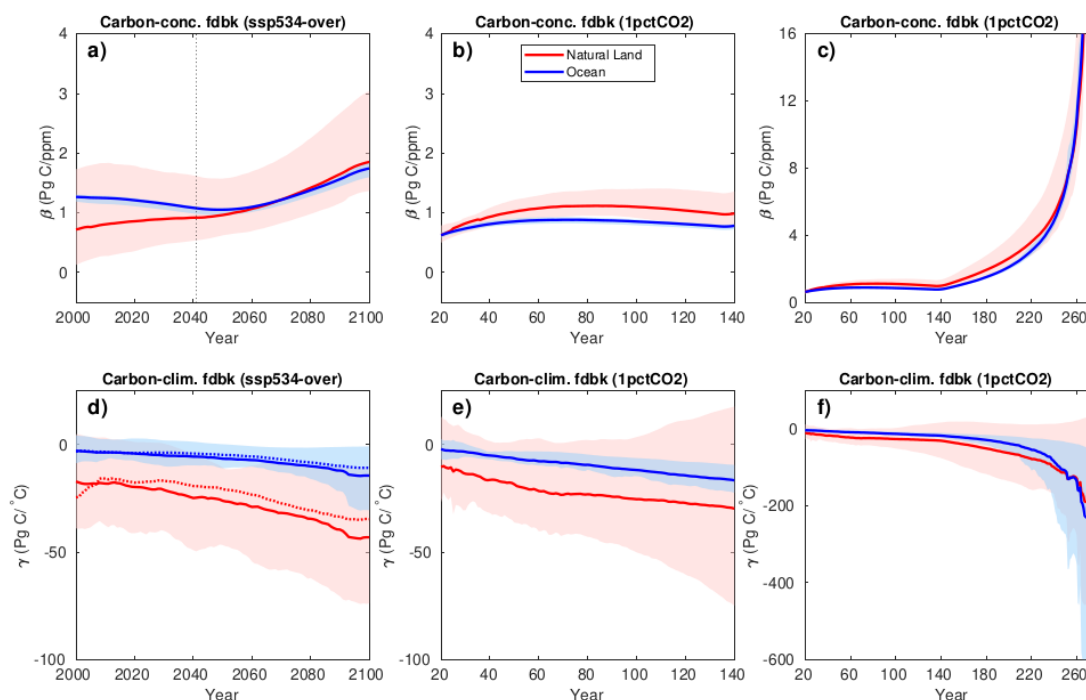
449

### 450 3.3 Carbon cycle feedback metrics

#### 451 3.3.1 Model mean global land and ocean responses

452 We now discuss the model-mean time evolution of the feedback metrics  $\beta$  and  $\gamma$  (Eqs. 1 and 2) derived  
 453 from the 1pctCO<sub>2</sub> and SSP5-3.4-OS simulations. In the SSP5-3.4-OS scenario (Fig. 5a) the model-mean  
 454 feedback metric  $\beta_L$  increases monotonically from about 0.7 to 1.9 PgC ppm<sup>-1</sup> during the period 2000-  
 455 2100. Over the ocean,  $\beta_O$  in the SSP5-3.4-OS scenario decreases slightly until the mid-21st century, and  
 456 then it rises to about 1.7 PgC ppm<sup>-1</sup>. Due to the much larger spread in carbon fluxes over land (Fig. 2),  
 457 the resulting model spread for both  $\beta_L$  and  $\gamma_L$  is also much larger than for  $\beta_O$  and  $\gamma_O$ .

458 For the 1pctCO<sub>2</sub> simulation, during the ramp-up phase over both land and ocean (Fig. 5b),  $\beta$  initially  
 459 increases and then decreases slightly with increasing [CO<sub>2</sub>] consistent with the results of Arora et al.  
 460 (2013) for the same experiment but using CMIP5 ESMs. In contrast, during the ramp-down phase of the  
 461 1pctCO<sub>2</sub>-cdr experiment,  $\beta$  reaches very high values over both land and ocean (Fig. 5c). This is because,  
 462 during the carbon removal phase of the 1pctCO<sub>2</sub>-cdr experiment, there is a much larger amount of  
 463 accumulated ocean and terrestrial carbon for the same atmospheric CO<sub>2</sub> concentration due to the large  
 464 hysteresis seen in Figs. 3 and 4. Eventually, while [CO<sub>2</sub>] is approaching pre-industrial values (i.e.,  $\Delta$ [CO<sub>2</sub>]  
 465 reaches zero), changes in cumulative fluxes (i.e., carbon stocks) relative to their pre-industrial values  
 466 remain positive, making  $\beta$  ill-defined towards the end of the 1pctCO<sub>2</sub> ramp-down. For the same reason,  
 467 an increase of  $\beta_L$  and  $\beta_O$  is also seen in the SSP5-3.4-OS scenario after the CO<sub>2</sub> concentration peak in  
 468 2062.



469





470 **Figure 5:** Model-mean  $\beta$  (a-c) and  $\gamma$  (d-f) feedback metrics in the SSP5-3.4-OS and 1pctCO2 experiments  
471 for natural land and ocean. Panels (b and e) show a zoom into the ramp-up phase of the time series  
472 shown on panels (c and f). Shadings show the range across the models. The dotted vertical line on panel  
473 a indicates where  $[\text{CO}_2]$  growth rate peaks in the fully coupled SSP5-3.4-OS experiment. Dotted curves  
474 on panel d indicate the model mean with the assumption of negligible temperature change in the BGC  
475 simulation. An 11-year moving average has been used in all panels.

476  
477 The model mean feedback factor  $\gamma$  is negative as the impact of climate change generally reduces the  
478 carbon stocks of land and ocean. In both SSP5-3.4-OS and 1pctCO2 experiments, the carbon-climate  
479 feedback is increasing over time (more negative  $\gamma$ , Fig. 5d and e), similar to figure 6 of Arora et al.  
480 (2013). The carbon-climate feedback is generally much smaller for the ocean than for land, and the  
481 model uncertainty for  $\gamma_O$  is only a small fraction of  $\gamma_L$ . Note that the same globally averaged surface air  
482 temperature anomaly is being used for the calculation of both  $\gamma_O$  and  $\gamma_L$  (Eq. 2). As noted above, the  
483 CanESM5 model simulates a globally increasing land uptake due to climate change towards the end of  
484 the 1pctCO2 simulation (Fig. 4e), resulting in a positive  $\gamma_L$  for this model. During the ramp-down phase  
485 of the 1pctCO2 experiment (Fig. 5f),  $\gamma$  reaches very large negative values. Similar to  $\beta$ , this is caused by  
486 the large hysteresis of the climate change impact on cumulative carbon stock while the surface  
487 temperature change becomes small (see Eq. 2). The assumption of  $\Delta T^{BGC} = 0$  generally works well  
488 except for  $\gamma_L$  in the SSP5-3.4-OS scenario where non- $\text{CO}_2$  forcings have a significant contribution to  
489  $\Delta T^{BGC}$  (dashed curves in Fig. 5d).

490 The global feedback factors  $B$  and  $\Gamma$  for the SSP5-3.4-OS and 1pctCO2 simulations are shown in Fig. S4.  
491 This feedback metric directly reflects the instantaneous fluxes, not cumulative fluxes, and is therefore  
492 less influenced by the history of carbon fluxes, unlike  $\beta$  and  $\gamma$ . Consistent with Fig. 2, the model-mean  
493  $B$  remains positive during the SSP5-3.4-OS simulation and during the positive emission phase of the  
494 1pctCO2 both over natural land and ocean. Only one model indicates a negative carbon-concentration  
495 feedback over natural land towards the very end of the SSP5-3.4-OS simulation during its relatively  
496 short negative emission phase.  $B$  reflects the saturation of carbon sinks in the 1pctCO2 simulation with  
497 time and decreases monotonically during the positive emission phase. Similar to what we have seen  
498 earlier for  $\beta$ ,  $B$  shows large but negative values towards the end of the 1pctCO2 ramp-down phase (Fig.  
499 S4c).

500 An interesting difference between the  $\gamma$  and  $\Gamma$  feedback metrics is seen towards the end of the 1pctCO2  
501 negative emissions phase (Fig. S4f), where  $\Gamma_L$  turns positive around year 180. This indicates that the land  
502 biosphere starts gaining carbon that was previously lost due to the impacts of climate change. In  
503 contrast,  $\Gamma_O$  remains negative indicating that the ocean continues to lose carbon due to warmer than  
504 pre-industrial conditions until the end of the 1pctCO2 ramp-down phase. Because they are based on  
505 cumulative emissions, both  $\gamma_O$  and  $\gamma_L$  remain negative throughout the 1pctCO2 ramp-down. This  
506 illustrates that the use of a feedback metric based on time-integrated carbon fluxes might obscure  
507 changes in important processes during net-negative emission phases. Eventually, both approaches for  
508 calculating feedback metrics become ill-defined when the deviation of  $[\text{CO}_2]$  or temperature from their  
509 pre-industrial values becomes small. This implies that both feedback metrics are not suited to describe



510 feedbacks towards the end (and beginning) of a concentration driven simulation set-up where pre-  
511 industrial concentrations are restored.

512

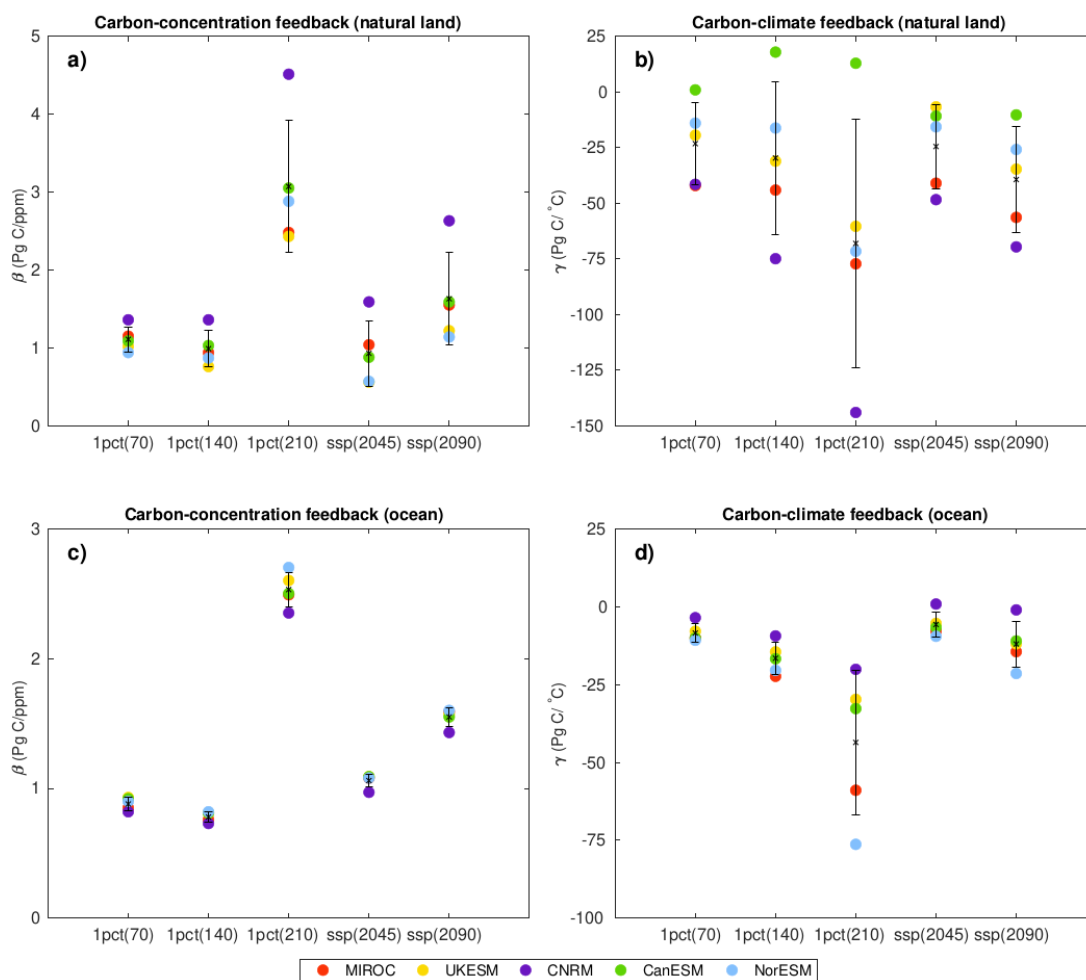
### 513 3.3.2 Model uncertainties and relative feedback strength in global feedback metrics

514 Figure 6 shows the model spread of feedback metrics at different points in time for the 1pctCO<sub>2</sub>  
515 simulation and the SSP5-3.4-OS scenario (see also Table 2). The larger model-mean values during the  
516 negative emission phases have been discussed in the previous section, but Fig. 6 also shows a strong  
517 increase in model uncertainty (measured as the standard deviation around the model mean, Table 2)  
518 between the ramp-up and ramp-down phase of the 1pctCO<sub>2</sub> simulation. For both  $\beta_L$  and  $\beta_O$ , there is  
519 either no ( $\beta_O$ ) or only a small ( $\beta_L$ ) increase in model uncertainty between the years 70 and 140 of the  
520 1pctCO<sub>2</sub> simulation, whereas at year 210 uncertainty has increased by about a factor of four. This  
521 “jump” in uncertainty in  $\beta$  is solely caused by differences in how the models react to the sharp change  
522 in forcing from increasing to decreasing CO<sub>2</sub> at year 140 (see Eq. 1, note that atmospheric CO<sub>2</sub> is  
523 prescribed and  $\Delta T^{BGC}$  is small). A similar behavior is seen for  $\gamma_O$ , while for  $\gamma_L$  the increase in model  
524 uncertainty is more gradual, i.e., the increase between years 70 and 140 is about the same as between  
525 years 140 and 210. There is also a consistent increase in model uncertainty in all feedback metrics from  
526 the positive to the negative emissions phase in the SSP5-3.4-OS scenario.

527 The relative strength of the feedback among the models remains relatively stable over time, between  
528 positive and negative emission phases, and between the different experiments. Model A having a  
529 stronger (weaker) feedback than model B at one of the instances depicted in Fig. 6, indicates that model  
530 A will have a stronger (weaker) feedback than model B for the other instances with only few exceptions.  
531 Most of these exceptions arise because modeled feedbacks are very similar such that small changes in  
532 feedback strength can lead to a different ranking. In a few cases relative feedback strength evolves  
533 differently in the models. For example, NorESM2-LM evolves from having a weaker than average  $\gamma_L$  in  
534 the positive emission phase of the 1pctCO<sub>2</sub> simulation to having a stronger than average  $\gamma_L$  in the  
535 negative emission phase.

536 Finally, it is worth noting that while the model uncertainty in  $\gamma_O$  is much smaller than in  $\gamma_L$  during the  
537 ramp-up phase of the 1pctCO<sub>2</sub> simulation (uncertainty in  $\gamma_O$  is only 15% of those in  $\gamma_L$  at year 140), this  
538 situation has changed for the ramp-down phase. At year 210, the uncertainty in the ocean carbon-  
539 climate feedbacks has grown much stronger than the uncertainties of the terrestrial carbon-climate  
540 feedback, such that model uncertainties in  $\gamma_O$  are 42% of those in  $\gamma_L$ .

541



542

543 **Figure 6:** Globally averaged values of  $\beta$  (a and c) and  $\gamma$  (b and d) feedback metrics in the 1pctCO<sub>2</sub> (years  
 544 70, 140, and 210) and SSP5-3.4-OS (years 2045 and 2090) experiments for natural land and ocean. The  
 545 bars show the mean  $\pm$  1 standard deviation range, and the individual colored dots represent individual  
 546 models.

547

548

549 **Table 2:** Globally averaged values of  $\beta$  (Pg C ppm<sup>-1</sup>) and  $\gamma$  (Pg C °C<sup>-1</sup>) feedback metrics at years 70, 140, and 210  
 550 of the 1pctCO<sub>2</sub> simulation and years 2045 and 2090 at the ramp-up and ramp-down phases of the SSP5-3.4-OS  
 551 experiment for natural land and ocean.

552

	MIROC-ES2L	UKESM1-0-LL	CNRM-ESM2-1	CanESM5	NorESM2-LM	Mean
$\beta_{L(70)}$	1.15	1.02	1.36	1.09	0.94	1.11 (SD=0.16)



$\beta_{L(140)}$	0.94	0.76	1.36	1.03	0.87	0.99 (SD=0.23)
$\beta_{L(210)}$	2.48	2.43	4.51	3.05	2.88	3.07 (SD=0.85)
$\beta_{L(2045)}$	1.04	0.56	1.59	0.88	0.57	0.93 (SD=0.42)
$\beta_{L(2090)}$	1.55	1.22	2.63	1.59	1.14	1.63 (SD=0.59)
$\gamma_{L(70)}$	-42.14	-19.54	-41.58	0.82	-14.12	-23.31 (SD=18.5)
$\gamma_{L(140)}$	-44.17	-31.19	-74.97	17.78	-16.31	-29.77 (SD=34.3)
$\gamma_{L(210)}$	-77.26	-60.45	-144.01	12.77	-71.64	-68.12 (SD=55.8)
$\gamma_{L(2045)}$	-41.08	-6.80	-48.46	-10.93	-15.78	-24.61 (SD=18.9)
$\gamma_{L(2090)}$	-56.43	-34.76	-69.66	-10.41	-25.95	-39.44 (SD=23.7)
$\beta_{O(70)}$	0.85	0.93	0.82	0.92	0.90	0.88 (SD=0.05)
$\beta_{O(140)}$	0.76	0.81	0.73	0.81	0.82	0.78 (SD=0.04)
$\beta_{O(210)}$	2.49	2.60	2.35	2.50	2.70	2.53 (SD=0.13)
$\beta_{O(2045)}$	1.08	1.09	0.97	1.09	1.08	1.06 (SD=0.05)
$\beta_{O(2090)}$	1.59	1.57	1.43	1.55	1.60	1.55 (SD=0.07)
$\gamma_{O(70)}$	-10.09	-7.95	-3.60	-10.13	-10.84	-8.52 (SD=2.96)
$\gamma_{O(140)}$	-22.40	-14.56	-9.44	-16.77	-20.48	-16.61 (SD=5.10)
$\gamma_{O(210)}$	-58.94	-29.78	-20.16	-32.75	-76.28	-43.59 (SD=23.2)
$\gamma_{O(2045)}$	-7.88	-5.43	0.78	-6.75	-9.56	-5.77 (SD=3.96)
$\gamma_{O(2090)}$	-14.50	-11.98	-1.10	-11.05	-21.50	-12.03 (SD=7.35)

553

554

555

### 3.3.3 Model differences in the terrestrial carbon-concentration feedback

556

557

558

559

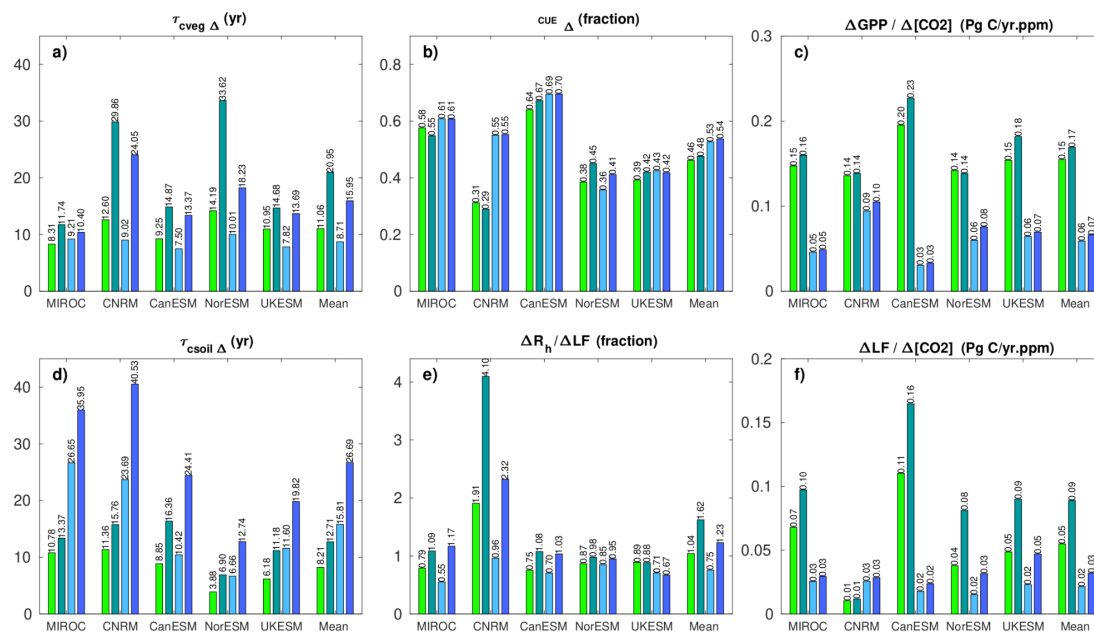
Figure 7 shows the individual components of the decomposition of  $\beta$  (Eq. 3), separately for tropical and subtropical (30°S-30°N) and higher latitudes (between 30°N/S and poles), both on the ramp-up and ramp-down phases (years 70 and 210, respectively) of the 1pctCO2-bgc experiment. The time periods are selected such that the atmospheric CO<sub>2</sub> concentration is the same (569 ppm, a doubling of pre-



560 industrial CO<sub>2</sub> concentration). All models consistently show increases in both  $\tau_{cveg\Delta}$  and  $\tau_{csoil\Delta}$  during  
561 the ramp-down compared to the ramp-up phase, since these metrics are based on cumulative  
562 vegetation and soil carbon (Eq. 3), which are slower than NPP and GPP in reacting to decreasing [CO<sub>2</sub>].  
563 Lower (higher) latitudes are associated with higher  $\tau_{cveg\Delta}$  ( $\tau_{csoil\Delta}$ ). Likewise, the litterfall term  $\frac{\Delta LF}{[CO_2]}$  is  
564 larger during the ramp-down phase in all models due to lagged reaction of vegetation carbon to the  
565 decrease in [CO<sub>2</sub>], with this effect being generally most pronounced at low latitudes. There is also a  
566 consistent but small increase in the term  $\frac{\Delta GPP}{[CO_2]}$ , which represents the CO<sub>2</sub> fertilization effect. This  
567 increase implicitly includes the effect of changes (typically an increase) in standing vegetation biomass  
568 and leaf area index for all models but also changes in vegetation cover as [CO<sub>2</sub>] varies for UKESM that  
569 simulates dynamic vegetation cover. For the dimensionless fractions  $\frac{\Delta R_h}{\Delta LF}$  and CUE<sub>Δ</sub>, changes between  
570 ramp-up and ramp-down phases are less consistent between the models. For CUE<sub>Δ</sub>, three models show  
571 an increase and two models a decrease, although the changes between ramp-up and ramp-down  
572 phases are generally small. For  $\frac{\Delta R_h}{\Delta LF}$  changes range from a 115% increase (CNRM at low latitudes) to a  
573 small decrease (UKESM). It is worth noting that for four out of six terms of Eq. 3 ( $\tau_{cveg\Delta}$ ,  $\tau_{csoil\Delta}$ ,  $\frac{\Delta R_h}{\Delta LF}$ ,  
574 and  $\frac{\Delta LF}{[CO_2]}$ ) the model disagreement is significantly larger during the ramp-down phase of the 1pctCO2  
575 simulation, indicating that changes in these processes are responsible for the strong increase in model  
576 uncertainty in  $\beta_L$  between positive and negative emission phases pointed out in the previous section.

577 The decomposition applied here helps to understand some of the model differences visible in Fig. 4. As  
578 already pointed out in Arora et al. (2020), the high accumulation of terrestrial carbon by the CNRM-  
579 ESM2-1 model in the BGC simulation (Fig. 4b) is not caused by a particularly strong CO<sub>2</sub> fertilization  
580 effect or CUE<sub>Δ</sub> but rather by relatively high values of  $\tau_{cveg\Delta}$  and  $\tau_{csoil\Delta}$ , indicating long residence  
581 timescales in vegetation and soil. Likewise, CanESM5's higher than average atmosphere-land C flux (Fig.  
582 4b), despite its near-average strength of the CO<sub>2</sub> fertilization effect and soil and vegetation turnover  
583 times is due to its high CO<sub>2</sub> fertilization effect at lower latitudes and also its high CUE<sub>Δ</sub> through which  
584 the model converts a much larger fraction of GPP to NPP. Compared to the other models, CanESM5  
585 also shows the largest relative increase (85% and 134% for lower and higher latitudes, respectively) in  
586  $\tau_{csoil\Delta}$  between years 70 and 210.

587  
588



589  
590  
591  
592  
593  
594  
595

**Figure 7:** Individual terms of Eq. (3) contributing to  $\beta_L$ . Values for tropical and subtropical (between 30°S and 30°N) regions are in green, and for northern latitudes (above 30°S and 30°N) are in blue. Lighter (darker) color on each panel corresponds to the middle of the ramp-up (ramp-down) phase of the 1pctCO<sub>2</sub>-bgc and 1pctCO<sub>2</sub>-cdr-bgc experiments (years 70 and 210, respectively).

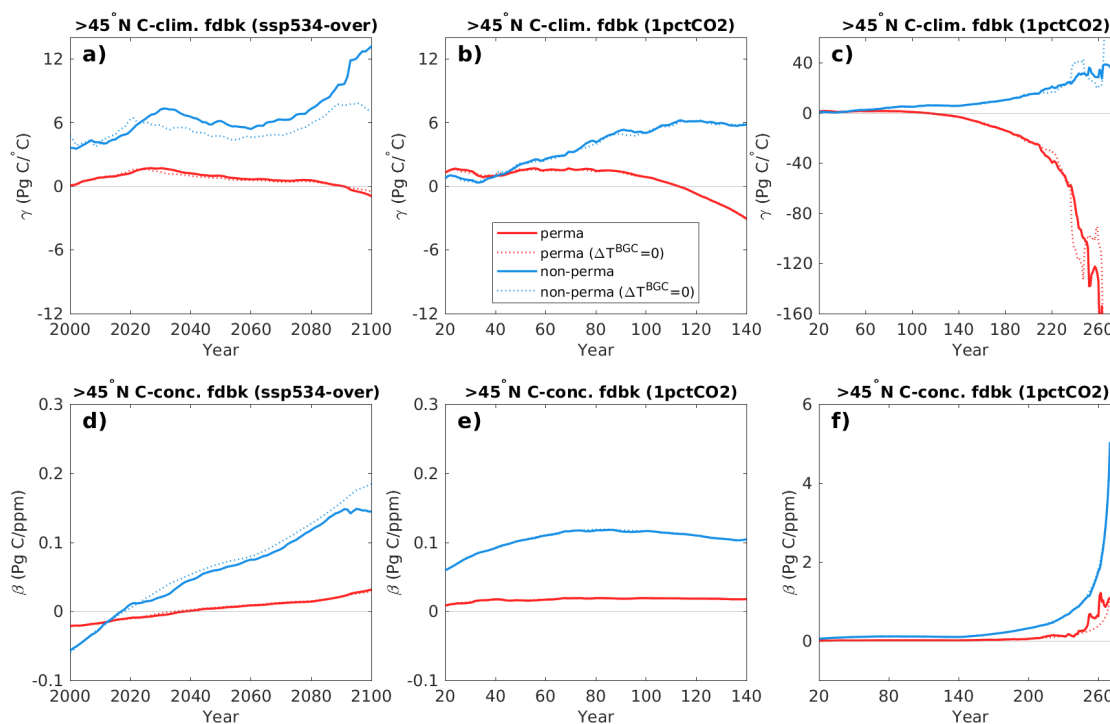
### 3.3.4 Northern hemisphere high-latitude permafrost and non-permafrost regions

Of the models considered here, only NorESM2-LM has a terrestrial model that vertically resolves soil carbon (CLM5, Lawrence et al. 2019). Since this is a prerequisite to skillfully simulate carbon release during gradual permafrost degradation, we restrict our analysis of high latitude and permafrost feedbacks to the NorESM2-LM model. If only natural land is considered, the area associated with permafrost and non-permafrost regions north of 45°N is about 14.7 and 17.5 x10<sup>6</sup> km<sup>2</sup>, respectively (total area is 14.7 and 24.1 x10<sup>6</sup> km<sup>2</sup>).

The effect of warming on carbon uptake in the high-latitude non-permafrost region is positive ( $\gamma > 0$ , increased uptake) in NorESM2-LM in both the SSP5-3.4-OS and 1pctCO<sub>2</sub> simulation (Fig. 8a-c, blue lines). Within the permafrost region,  $\gamma$  is close to zero for the SSP5-3.4-OS simulation up to 2100 and the ramp-up phase of the 1pctCO<sub>2</sub> simulation (Fig. 8a,b, red line), albeit with a decreasing (more negative) trend. This is due to a compensation of vegetation carbon gain and soil carbon losses (Fig. S5). During the ramp-down phase of the 1pctCO<sub>2</sub> simulation, permafrost soil carbon losses increase approximately until year 210 of the simulation (Fig. S5). Thereafter, permafrost soil carbon stays roughly constant with a cumulative loss of about 55 PgC over the simulation. Vegetation carbon over the permafrost region still increases for the first 30 years of the ramp-down phase of the 1pctCO<sub>2</sub>



612 simulation, after which it decreases mainly due to decreasing temperature (Fig. S5g). The  $\gamma$  value  
 613 calculated for the permafrost region, therefore, shows a sharp decrease during the ramp-down period  
 614 of the 1pctCO2 simulation (Fig. 8c). Eventually, when  $\Delta T$  approaches small values  $\gamma$  loses its significance  
 615 as seen before for the global feedback factors.



616

617 **Figure 8:**  $\gamma$  (a-c) and  $\beta$  (d-f) for northern hemisphere high latitude natural land permafrost and non-  
 618 permafrost regions in the SSP5-3.4-OS and 1pctCO2 simulations using the NorESM model. An 11-year  
 619 moving average has been used in all panels.

620

621 In both the SSP5-3.4-OS scenario and the 1pctCO2 simulations,  $\beta$  is positive (except initially in the SSP5-  
 622 3.4-OS simulation) although the absolute values remain very small. The carbon-concentration feedback  
 623 is stronger over the non-permafrost area, where both soil and vegetation carbon increase in the BGC  
 624 simulation, than over the permafrost area, where soil and vegetation carbon stay almost constant in  
 625 BGC (Fig. S5).

626 NorESM2-LM has the smallest transient climate response (TCR) of the models considered here, and it  
 627 can be expected that the permafrost carbon-climate feedback estimated here would be larger in a  
 628 model with higher TCR. Nevertheless, the permafrost carbon loss of 26.9 Pg C °C<sup>-1</sup> in the year 210 of the  
 629 simulation contributes 38% of the total carbon-climate feedback at this point in time in NortESM2-LM.

630



### 631 3.4 Geographical pattern of carbon cycle feedback metrics

632 We have calculated  $\beta$  and  $\gamma$  feedback factors at grid-scale to assess the spatial patterns of feedbacks  
633 over the land and ocean (Figs. 9 and 10). In order to compare positive and negative emission phases,  
634 we selected 21-year time intervals centered at years 70 and 210 of the ramp-up and ramp-down phases  
635 of the 1pctCO<sub>2</sub> simulation, at an atmospheric CO<sub>2</sub> concentration of 570 ppm (corresponding to a  
636 doubling of pre-industrial CO<sub>2</sub> concentration). We also selected a 21-year time-interval centered at year  
637 2045 (corresponding to CO<sub>2</sub> concentration of 523 ppm), shortly before the CO<sub>2</sub> peak of the SSP5-3.4-  
638 OS scenario. We have also analyzed a 21-year time interval during the net-negative emission phase of  
639 the SSP scenario (centered at year 2090), but since the time-period of net-negative emissions in the  
640 SSP-scenario is relatively short, we focus on comparing the feedbacks during the positive and negative  
641 emission phases of the 1pctCO<sub>2</sub> simulation alongside with the feedbacks during the positive emission  
642 phase of SSP5-3.4-OS. For completeness, Fig. S6 shows the spatially resolved feedback during the net-  
643 negative emission phase of SSP5-3.4-OS.

644 In the 1pctCO<sub>2</sub> simulation, rising [CO<sub>2</sub>] increases the modeled carbon sinks almost everywhere (i.e.,  
645 positive  $\beta$ ) over the land and ocean (Fig. 9a-e). CanESM5 shows a weak negative  $\beta$  over northern high-  
646 latitude land areas, and there are some spurious negative values of  $\beta$  over desert areas in some models.  
647 For the ocean, all models agree that the regions with the strongest increase of the oceanic CO<sub>2</sub> sinks in  
648 response to higher [CO<sub>2</sub>] are the North Atlantic and the Southern Ocean. As seen for the global average  
649 (Fig. 5),  $\beta$  remains positive and increases in magnitude during the ramp-down phase (Fig. 9 f-j, note the  
650 different color scale). As an overarching observation, the large scale patterns of the carbon-  
651 concentration feedback are remarkably similar during the ramp-up and ramp-down phases of the  
652 1pctCO<sub>2</sub> simulation (with spatial correlations, averaged across all the models, of 0.93 and 0.80 over  
653 land and the ocean, respectively) but the magnitude of the feedback is about two times larger in the  
654 ramp-down phase, consistent with the lagged response of cumulative carbon uptake to the decrease  
655 in atmospheric CO<sub>2</sub> (Figs. 3 and 4). The most prominent change in the spatial pattern of  $\beta$  occurs in  
656 the equatorial Pacific. All models consistently show that this area has turned from a cumulative carbon  
657 sink at year 70 to a cumulative carbon source at year 210.

658 We find the largest values of  $\beta$  over tropical land and to a lesser extent over northern hemisphere  
659 temperate and boreal ecosystems coincident with areas of large biomass (forests). For three of the  
660 models (NorESM2-LM, CanESM5, and UKESM1-0-LL), the feedback is clearly dominated by tropical and  
661 subtropical regions, while for MIROC-ES2L the feedback is approximately of the same strength in  
662 northern temperate and high-latitude regions. For CNRM-ESM2-1, the carbon-concentration feedback  
663 is on average stronger north of 30° latitude than in tropical/subtropical regions. For NorESM2-LM and  
664 UKESM1-0-LL, the tropical dominance of the carbon-concentration feedback stems from vegetation  
665 carbon, while for CanESM5 both vegetation and soil carbon contribute about equally (Figs. S7 and S8).

666 The results presented in Section 3.3.3 provide to some extent a mechanistic understanding of these  
667 model differences. CNRM-ESM2-1 has the highest CO<sub>2</sub> fertilization effect  $\frac{\Delta GPP}{[CO_2]}$  in high latitudes and





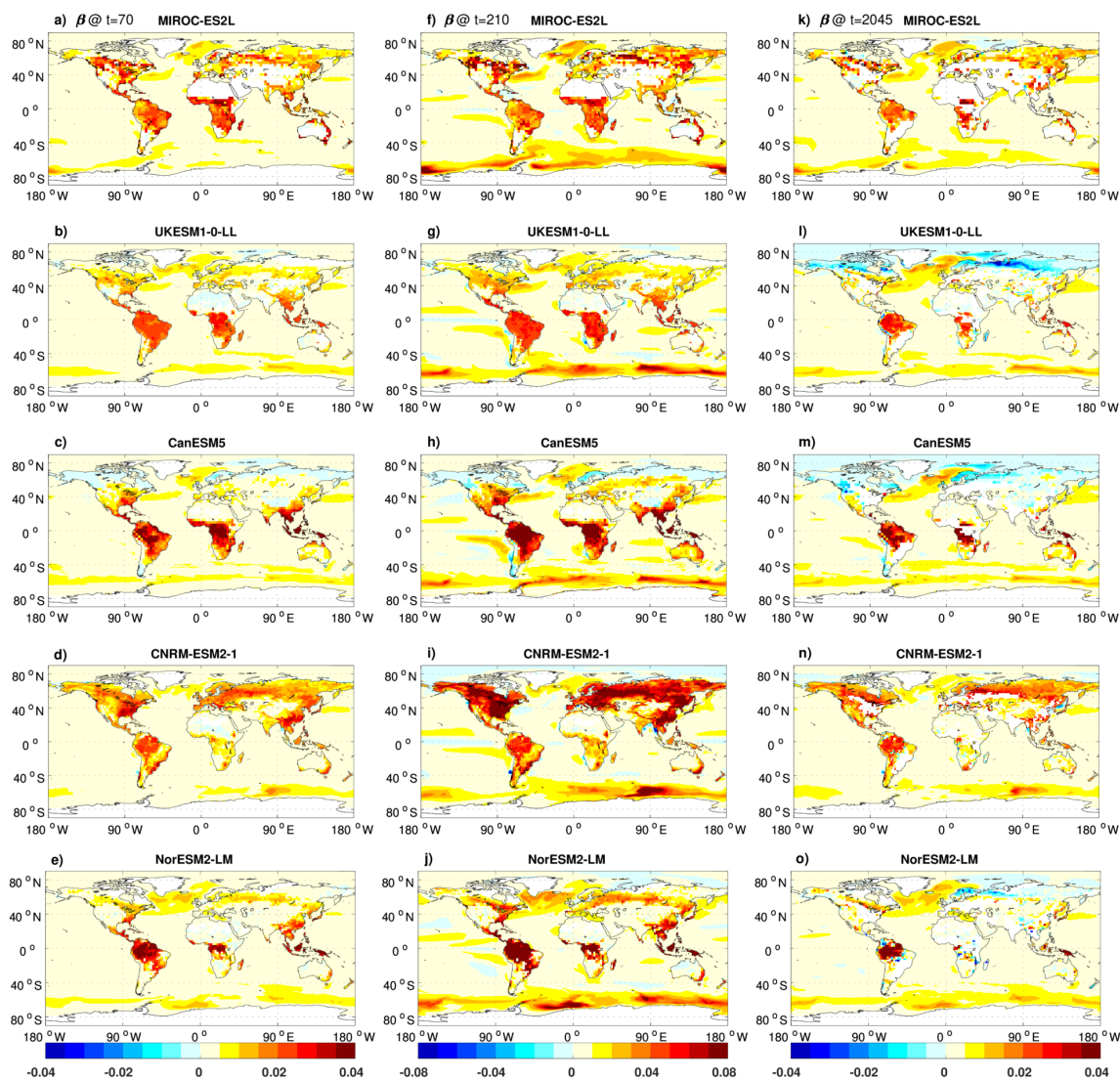
668 the lowest  $CUE\Delta$  at low latitudes. This, combined with a large high-latitude  $\tau_{csoil\Delta}$  leads to a larger  
669 carbon accumulation in vegetation and soil in higher latitudes than in the tropics/subtropics in this  
670 model. The three models with tropical dominance of  $\beta$  (NorESM2-LM, CanESM5, and UKESM1-0-LL)  
671 have a relatively high  $\tau_{cveg\Delta}$  and relatively low  $\tau_{csoil\Delta}$ . CanESM5, shows the strongest  
672 tropical/subtropical  $CO_2$  fertilization effect, but also a large response of the litterfall term leading to  
673 large responses in both vegetation and soil carbon.

674 In the SSP5-3.4-OS simulation, the ocean  $\beta$  magnitude is similar to that of the 1pctCO2 simulation and  
675 the spatial distribution of the ocean response to the  $[CO_2]$  rise is roughly consistent between the models  
676 (Fig. 9k-o). In contrast, the feedback pattern over natural land is different in some regions and models  
677 between the SSP scenario simulation and the idealized 1pctCO2 experiment. UKESM1-0-LL, CanESM5,  
678 and to a lesser extent NorESM2-LM project negative  $\beta$  values in some northern high latitude regions  
679 (e.g., Siberia). These negative  $\beta$  values are either not seen at all (UKESM1-0-LL, NorESM2-LM) or are  
680 weaker (CanESM5) in the 1pctCO2 simulation, and they originate from a combination of vegetation and  
681 soil carbon pools (Figs. S7 and S8). Unlike in the 1pctCO2 experiment, temperature changes are not  
682 negligible in the BGC simulation of the SSP5-3.4-OS experiment (Fig. 1). Nevertheless, the spatial  
683 distribution of the feedback factor  $\beta$  calculated with the assumption  $\Delta T^{BGC} = 0$  results in a similar  
684 pattern (not shown), which suggests that the non-negligible temperature changes in the BGC simulation  
685 are not the cause for these negative values of  $\beta$ . Rather, these negative values are most likely caused  
686 by remaining land use change in grid cells that we have classified as “natural” land with our simple  
687 threshold approach. This is consistent with the fact that the high-latitude negative  $\beta$  values occur in  
688 those models that have low  $\beta$  in these regions in the 1% simulation (i.e., a relatively small land use  
689 change perturbation can change  $\beta$  from positive to negative).

690

691

692



693  
694  
695  
696  
697  
698  
699

**Figure 9:** The spatial distribution of  $\beta$  ( $\text{kg C m}^{-2} \text{ppm}^{-1}$ ) at year 70 of the ramp-up phase of the 1pctCO<sub>2</sub> simulation (a-e), at year 210 of the ramp-down phase of the 1pctCO<sub>2</sub> simulation (f-j), and at year 2045 (natural land only, white areas are crop-dominated grid cells) during the positive emission phase of the SSP5-3.4-OS scenario (k-o).

700  
701  
702  
703  
704

Figure 10 indicates that the ESMs considered here simulate predominantly negative values of  $\gamma_o$  over the ocean. Positive values of  $\gamma_o$  are found in the Arctic, and in some cases in parts of the polar Southern Ocean adjacent to Antarctica. Climate change increases the ocean CO<sub>2</sub> sink in these regions mainly due to a reduction in sea ice coverage (Roy et al. 2011; Schwinger et al. 2014). The North Atlantic Ocean and the Southern Ocean have the largest negative  $\gamma_o$  values due to changes in ocean circulation and



705 deep water formation. In tropical and subtropical ocean regions, the reduced oceanic carbon uptakes  
706 can be attributed to warming-induced decreased CO<sub>2</sub> solubility and increased stratification (Roy et al.  
707 2011).

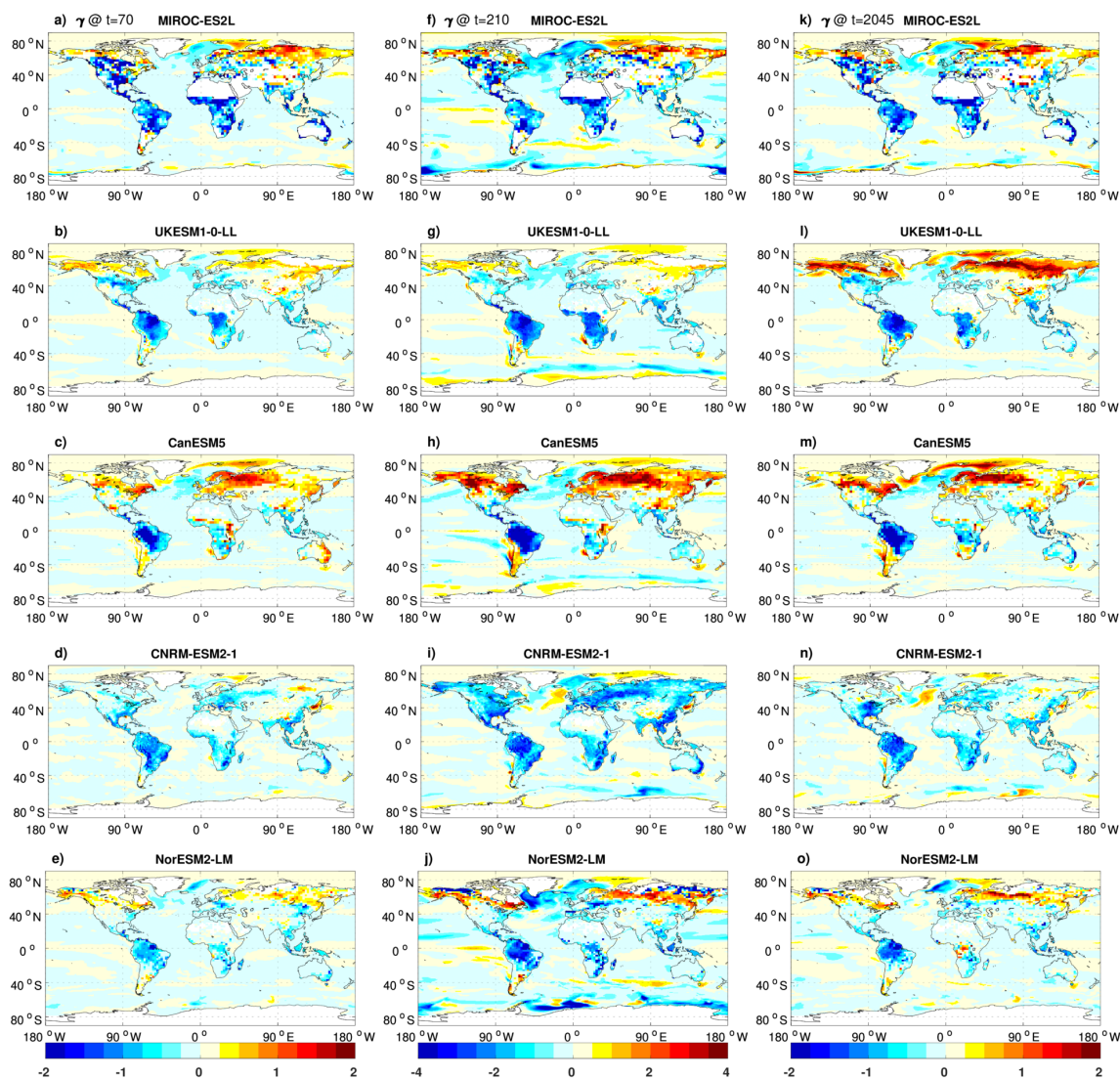
708 Over land, climate change generally reduces carbon sinks in the tropics and mid-latitudes. In the high  
709 latitudes models disagree on the strength and the sign of the carbon-climate feedback. CNRM-ESM2-1  
710 shows relatively strong soil carbon losses in northern high latitudes, which overcome vegetation carbon  
711 gains (Fig. S9 and S10) leading to mostly negative values of  $\gamma_L$  in this region. As mentioned above,  
712 CanESM5's carbon-climate feedback switches from weak negative at 2xCO<sub>2</sub> to positive at 4xCO<sub>2</sub>. Figure  
713 9c clearly shows that the positive global  $\gamma$  values originate from the northern hemisphere high latitudes.  
714 Also, the positive  $\gamma_L$  in CanESM5 over the northern high latitudes is seen in both vegetation and soil  
715 carbon reservoirs, but with a time lag for soil carbon. Consistent with our analysis in Sect. 3.3.4,  
716 NorESM2-LM shows permafrost carbon loss in north-eastern Siberia and northern Alaska, but these  
717 losses become significant only during the ramp-down phase of the 1pctCO<sub>2</sub> simulation (Fig. 9j).

718 The spatial pattern of the carbon-climate feedback is similar during the ramp-up and ramp-down phases  
719 of the 1pctCO<sub>2</sub> simulation, but the magnitude has roughly doubled during the ramp-down phase,  
720 consistent with the cumulative nature of the  $\gamma$  feedback metric used here (note the different color-  
721 scales in Fig. 9). The correlations of the spatial patterns (at years 70 and 210) are lower than for  $\beta$  and  
722 range from 0.41 (MIROC-ES2L) to 0.66 (UKESM1-0-LL) for  $\gamma_O$  and from 0.49 (NorESM2-LM) to 0.88  
723 (UKESM1-0-LL) for  $\gamma_L$ .

724 The value of the  $\gamma$  feedback metric in the SSP5-3.4-OS scenario simulation is less affected by land-use  
725 change, since the same land-use changes are imposed in both the COU and the BGC simulation. In  
726 contrast to  $\beta$ , which is directly altered by carbon stock changes due to land-use changes,  $\gamma$  is only  
727 influenced indirectly, possibly by different sensitivities of the new vegetation cover after a land-use  
728 transition, or by changes in local to regional climatic conditions. In the global mean, the carbon-climate  
729 feedback during the positive emission phase is very similar for the SSP scenario and the 1pctCO<sub>2</sub>  
730 simulation (Fig. 5d and e). Also, the spatial patterns of  $\gamma_L$  are largely similar between the SSP5-3.4-OS  
731 and the ramp-up phase of the 1pctCO<sub>2</sub> simulation with correlations ranging from 0.71 (NorESM2-LM)  
732 to 0.84 (CNRM-ESM2-1). The largest difference between the two simulations is an enhanced positive  
733 feedback over northern high-latitude land in the UKESM1-0-LL model in SSP scenario compared to the  
734 1pctCO<sub>2</sub> simulation, which is seen in both vegetation and soil carbon pools (Figs. S9 and S10).

735 Over the ocean the global mean carbon-climate feedback is slightly smaller in SSP5-3.4-OS compared  
736 to the 1pctCO<sub>2</sub> simulation (Fig. 3f), but again, the spatial pattern is largely similar with correlations  
737 ranging from 0.47 (CNRM-ESM2-1) to 0.78 (MIROC-ES2L).

738



739

740

741

742

743

**Figure 10:** same as Fig. 9 but for  $\gamma$  ( $\text{kg C m}^{-2} \text{ } ^\circ\text{C}^{-1}$ ). Note that cropland areas are not excluded from panels (k-o) as in Fig. 9.

744

745

746

747

748

749

750

#### 4. Summary and conclusions

We have investigated carbon cycle feedbacks in a highly idealized model experiment with exponentially increasing and decreasing atmospheric  $\text{CO}_2$  concentration (1pct $\text{CO}_2$ ) and in a more realistic overshoot scenario simulation (SSP5-3.4-OS). We employ an ensemble of five CMIP6 ESMs that have run additional (biogeochemically coupled) simulations that allow us to separate the effects of changing atmospheric  $\text{CO}_2$  and of changing surface climate on the simulated carbon cycle. We discuss global mean carbon fluxes and employ the widely used carbon cycle feedback metrics of  $\beta$  and  $\gamma$  (Friedlingstein et al. 2003) to compare feedbacks between models and between phases of (implied) positive and negative  $\text{CO}_2$



751 emissions as well as the (model) uncertainty of these feedbacks. To determine the sources of  
752 uncertainty for the terrestrial carbon-concentration feedback, we also decompose  $\beta_L$  into contributions  
753 from different processes following the methodology of Arora et al. (2020), and investigate spatial  
754 feedback patterns and their changes.

755 We find that both the carbon-concentration ( $\beta$ ) and the carbon-climate ( $\gamma$ ) feedbacks show a  
756 considerable hysteresis behavior during negative emission phases. Hysteresis is stronger for the ocean  
757 relative to the strength of the feedbacks, although the hysteresis of the terrestrial carbon cycle  
758 feedbacks is larger in absolute terms. The well-known reduction of ocean and land carbon uptake with  
759 increasing temperatures continues long into the negative emissions phases of the simulations (when  
760 temperature is decreasing), albeit at a reduced rate. For the ocean, there is still a reduction in carbon  
761 stocks due to legacy warming when pre-industrial atmospheric CO<sub>2</sub> is restored in the 1pctCO<sub>2</sub>  
762 simulation, consistent with the single-model studies of Schwinger and Tjiputra (2018) and Bertini and  
763 Tjiputra (2022). In contrast, all models agree that the effect of legacy warming is less important for the  
764 terrestrial carbon-climate feedback as the reduction of global mean surface temperature leads to a  
765 reduction in temperature-induced losses of terrestrial carbon towards the end of the 1pctCO<sub>2</sub>  
766 simulation.

767 It is well known that carbon cycle feedback metrics vary over time, and between different scenarios.  
768 Here we find that when (implied) emissions change from positive to negative,  $\beta$  and  $\gamma$  (defined  
769 according to Friedlingstein et al. 2003) show an increase in absolute values due to the large hysteresis  
770 of carbon stock changes, while temperature and atmospheric CO<sub>2</sub> decrease. Particularly, if the  
771 deviations in surface temperature and atmospheric CO<sub>2</sub> become small towards the end of a modeled  
772 negative emission scenario, the magnitude of these feedback metrics “explodes” since they are defined  
773 as the ratio between the deviations in carbon stocks and the change in temperature and atmospheric  
774 CO<sub>2</sub>, respectively. Arguably, the latter is mainly a problem due to the strongly idealized simulation  
775 design of the 1pctCO<sub>2</sub> experiment, not for more realistic scenarios as the SSP5-3.4-OS. The feedback  
776 metrics B and  $\Gamma$  (defined according to Boer and Arora, 2009), which are based on instantaneous fluxes,  
777 also become ill-defined when deviations of surface temperature and atmospheric CO<sub>2</sub> approach zero,  
778 but unlike the  $\beta$  and  $\gamma$  feedback metrics, they are only indirectly affected by the history of carbon fluxes.  
779 These metrics thus respond faster to changes in atmospheric CO<sub>2</sub> concentration or temperature, for  
780 example, B clearly shows the point in time when carbon fluxes reverse and the land or ocean turn from  
781 a sink to a source of carbon under negative emissions.

782 We find that the relative strength of the feedback remains relatively robust between positive and  
783 negative emission phases and between the different simulations considered here. For example, a model  
784 with a stronger than average terrestrial carbon-concentration feedback ( $\beta_L$ ) during the positive  
785 emission phase of the 1pctCO<sub>2</sub> simulation will also show a stronger than average  $\beta_L$  during the negative  
786 emission phase or for the SSP5-3.4-OS scenario. Regarding the model uncertainty of feedback metrics  
787 we find that there is an increase in uncertainty in all feedback metrics between the positive and  
788 negative emission phases of the 1pctCO<sub>2</sub> simulation. Except for  $\gamma_L$ , this increase is much larger than  
789 expected from an accumulation of uncertainty over time. This indicates that there is an additional  
790 component of model uncertainty resulting from uncertainties in the model responses to the change  
791 from increasing to decreasing radiative forcing.



792 The geographical patterns of terrestrial  $\beta$  and  $\gamma$  feedback metrics highlight differences in the responses  
793 of tropical/subtropical versus temperate/boreal ecosystems as a major source of model disagreement.  
794 For individual models, however, the spatial feedback patterns are remarkably similar during phases of  
795 increasing CO<sub>2</sub> compared to phases of decreasing CO<sub>2</sub> concentrations, indicating that the increase of  
796 global mean values of  $\beta$  and  $\gamma$  during negative emissions phases does not stem from a particular region  
797 but is generally seen over the whole globe. We estimate the contribution of permafrost carbon release  
798 to the carbon-climate feedback only for one of the five ESMs (NorESM2-LM, which vertically resolves  
799 soil carbon). Permafrost carbon release is clearly seen as a strong negative feedback over the  
800 permafrost area, but it emerges only relatively late in the simulations. Permafrost carbon release  
801 accounts for 38% of NorESM2-LM's carbon-climate feedback at the midpoint of the negative emission  
802 phase of the 1pctCO<sub>2</sub> simulation. NorESM2 has the lowest transient climate response of the ESMs  
803 considered here and we therefore expect that other models might show an earlier and larger  
804 permafrost carbon release.

805 In the SSP5-3.4-OS simulation, the presence of land-use change complicates the analysis of feedbacks.  
806 Land-use change is not a feedback process, yet owing to the C4MIP simulation design, carbon losses (or  
807 gains) due to land use change are confounded with the carbon-concentration feedback derived from a  
808 biogeochemically coupled scenario simulation. If we disregard agricultural areas, terrestrial carbon  
809 cycle feedback patterns in the SSP5-3.4-OS scenario are largely similar to those in the 1pctCO<sub>2</sub>  
810 simulation.

811 We conclude with some recommendations for future research and the design of future model  
812 intercomparison projects (MIPs) like C4MIP and CDRMIP. We expect that understanding and reducing  
813 the large uncertainties in the response of ESMs to changes in atmospheric CO<sub>2</sub> and surface climate,  
814 particularly during phases of negative emissions, remains a research topic of high relevance. Here, we  
815 have shown that the uncertainties (model disagreement) in feedback metrics increases during phases  
816 of negative emissions, and that this increase, for most of the feedback metrics, cannot be explained by  
817 a linear accumulation of uncertainty with progressing simulation time. Identifying and better  
818 understanding the causes of such increased model disagreement under negative emissions should be  
819 pursued further with high priority.

820 Both the integrated-flux ( $\beta$  and  $\gamma$ ) and instantaneous-flux ( $B$  and  $\Gamma$ ) based feedback metrics were  
821 designed at a time when nearly all future climate change scenarios were characterized by continuously  
822 increasing atmospheric CO<sub>2</sub>. Indeed both metrics perform well for such scenarios and have allowed us  
823 to compare the strength of carbon-concentration and carbon-climate feedbacks across models, albeit  
824 with their well-known caveats (e.g., their scenario dependence). However, in scenarios where  
825 atmospheric CO<sub>2</sub> concentration decreases, these metrics become difficult to interpret, particularly in  
826 the extreme case when atmospheric CO<sub>2</sub> concentration and surface temperature approach their pre-  
827 industrial level. In the light of the discussion around CDR perhaps it is timely to rethink other but related  
828 forms of these metrics that describe the response of land and ocean carbon systems in scenarios of  
829 decreasing atmospheric CO<sub>2</sub> in a more robust manner.

830 The 1pctCO<sub>2</sub> simulation combined with the 1pctCO<sub>2</sub>-cdr simulation is an extremely idealized model  
831 experiment with huge (and infeasible) amounts of implied net-negative emissions and a discontinuity



832 at year 140, where implied emissions jump from large positive to large negative values. As we know  
833 that carbon cycle feedbacks are scenario dependent, it would be preferable to assess these feedbacks  
834 using model simulations that have a more realistic emission pathway and that include more realistic  
835 amounts of net-negative emissions. Alternative idealized simulation designs that include negative  
836 emissions have been proposed in the literature (MacDougall 2019; Schwinger et al. 2022) and we have  
837 also considered the SSP5-3.4-OS scenario in this study. However, the presence of land-use change and  
838 variable non-CO<sub>2</sub> forcings in SSP scenarios complicates the quantification of carbon cycle feedbacks.  
839 Whether this problem can be solved for future phases of C4MIP by providing more detailed model  
840 output or by requesting additional idealized experiments should be discussed in the C4MIP community.

841 Finally, most proposed negative emission options would be realized by manipulating the terrestrial or  
842 oceanic carbon sinks (e.g., bioenergy with carbon capture and storage, afforestation or ocean  
843 alkalization), thereby not only changing the atmospheric CO<sub>2</sub> concentration and possibly the surface  
844 climate but also the carbon cycle feedbacks themselves. Such interactions go beyond what can be  
845 addressed with the traditional C4MIP design of fully- and biogeochemically coupled ESM simulations.  
846 Consequently, a new framework for determining feedbacks in realistic scenarios of CDR deployment is  
847 needed and should be developed in close collaboration with the integrated assessment modeling  
848 community that will create such scenarios.

849

850

851

#### 852 **Data availability**

853 All CMIP6 model output data is freely available through the Earth System Grid Federation (for example,  
854 under <https://esgf-data.dkrz.de/search/cmip6-dkrz/>). The model output data of the 1pctCO2-cdr-bgc  
855 simulation will be made publicly available upon final acceptance of this manuscript.

856

857

#### 858 **Competing interests**

859 None of the authors has any competing interests.

860

861

#### 862 **Acknowledgements**

863 A.A., J.S., and H.L. were supported by the Research council of Norway through the project IMPOSE  
864 (grant no. 294930). J.S. and H.L. also received funding from the European Union's Horizon Europe  
865 research and innovation programme (project RESCUE, grant agreement no. 101056939).  
866 Supercomputing and storage resources for additional NorESM2 simulations were provided by UNINETT  
867 Sigma2 (projects nn9708k/ns9708k). T.H. was supported by the Integrated Research Program for  
868 Advancing Climate Models (TOUGOU, grant number JPMXD0717935715) and the Program for the  
869 Advanced Studies of Climate Change Projection (SENTAN, grant number JPMXD0722681344) from the



870 Ministry of Education, Culture, Sports, Science and Technology (MEXT), Japan. C.D.J. and S.L. were  
871 supported by the Joint UK BEIS/Defra Met Office Hadley Centre Climate Programme (GA01101), and  
872 the European Union's Horizon 2020 research and innovation programme under Grant Agreement No  
873 101003536 (ESM2025 - Earth System Models for the Future). R.S. and Y.S.-F. are grateful for the support  
874 of the team in charge of the CNRM-CM climate model. Supercomputing time was provided by the  
875 Meteo-France/DSI supercomputing center. R.S. acknowledges the European Union's Horizon 2020  
876 research and innovation program under grant agreement No. 101003536 (ESM2025 – Earth System  
877 Models for the Future). Y.S.-F. acknowledges the TRIATLAS project under the grant agreement No  
878 817578 and the COMFORT project under the grant agreement No 820989.

879

880 We acknowledge the World Climate Research Programme, which, through its Working Group on  
881 Coupled Modelling, coordinated and promoted CMIP6. We thank the climate modeling groups for  
882 producing and making available their model output, the Earth System Grid Federation (ESGF) for  
883 archiving the data and providing access, and the multiple funding agencies who support CMIP6 and  
884 ESGF.

885

886 The work reflects only the authors' view; the European Commission and their executive agency are  
887 not responsible for any use that may be made of the information the work contains.

888

889

890

## 891 References

- 892 Armstrong McKay, D. I., and Coauthors, 2022: Exceeding 1.5°C global warming could trigger multiple  
893 climate tipping points. *Science*, **377**, eabn7950, <https://doi.org/10.1126/science.abn7950>.
- 894 Arora, V. K., and Coauthors, 2013: Carbon–Concentration and Carbon–Climate Feedbacks in CMIP5  
895 Earth System Models. *J. Clim.*, **26**, 5289–5314, <https://doi.org/10.1175/JCLI-D-12-00494.1>.
- 896 ———, and Coauthors, 2020: Carbon–concentration and carbon–climate feedbacks in CMIP6 models  
897 and their comparison to CMIP5 models. *Biogeosciences*, **17**, 4173–4222,  
898 <https://doi.org/10.5194/bg-17-4173-2020>.
- 899 Bertini, L., and J. Tjiputra, 2022: Biogeochemical Timescales of Climate Change Onset and Recovery  
900 in the North Atlantic Interior Under Rapid Atmospheric CO<sub>2</sub> Forcing. *J. Geophys. Res. Oceans*,  
901 **127**, e2021JC017929, <https://doi.org/10.1029/2021JC017929>.
- 902 Boer, G. J., and V. Arora, 2009: Temperature and concentration feedbacks in the carbon cycle.  
903 *Geophys. Res. Lett.*, **36**, <https://doi.org/10.1029/2008GL036220>.
- 904 Boucher, O., and Coauthors, 2012: Reversibility in an Earth System model in response to CO<sub>2</sub>  
905 concentration changes. *Environ. Res. Lett.*, **7**, 024013, <https://doi.org/10.1088/1748-9326/7/2/024013>.
- 907 Canadell, J. G., and Coauthors, 2021: Global carbon and other biogeochemical cycles and feedbacks.  
908 *Climate Change 2021: The Physical Science Basis. Contribution of Working Group I to the*  
909 *Sixth Assessment Report of the Intergovernmental Panel on Climate Change*, V. Masson-  
910 Delmotte et al., Eds., Cambridge University Press.
- 911 Ciais, P., and Coauthors, 2013: Carbon and other biogeochemical cycles. *Climate Change 2013: The*  
912 *Physical Science Basis. Contribution of Working Group I to the Fifth Assessment Report of the*  
913 *Intergovernmental Panel on Climate Change*, Cambridge University Press, 465–570.





- 914 Eyring, V., S. Bony, G. A. Meehl, C. A. Senior, B. Stevens, R. J. Stouffer, and K. E. Taylor, 2016:  
915 Overview of the Coupled Model Intercomparison Project Phase 6 (CMIP6) experimental design  
916 and organization. *Geosci. Model Dev.*, **9**, 1937–1958, [https://doi.org/10.5194/gmd-9-1937-](https://doi.org/10.5194/gmd-9-1937-2016)  
917 2016.
- 918 Feng, J., and Coauthors, 2020: Warming-induced permafrost thaw exacerbates tundra soil carbon  
919 decomposition mediated by microbial community. *Microbiome*, **8**, 3,  
920 <https://doi.org/10.1186/s40168-019-0778-3>.
- 921 Friedlingstein, P., J.-L. Dufresne, P. M. Cox, and P. Rayner, 2003: How positive is the feedback  
922 between climate change and the carbon cycle? *Tellus B Chem. Phys. Meteorol.*, **55**, 692–700,  
923 <https://doi.org/10.3402/tellusb.v55i2.16765>.
- 924 —, and Coauthors, 2006: Climate–Carbon Cycle Feedback Analysis: Results from the C4MIP  
925 Model Intercomparison. *J. Clim.*, **19**, 3337–3353, <https://doi.org/10.1175/JCLI3800.1>.
- 926 Gasser, T., and Coauthors, 2018: Path-dependent reductions in CO<sub>2</sub> emission budgets caused by  
927 permafrost carbon release. *Nat. Geosci.*, **11**, 830–835, [https://doi.org/10.1038/s41561-018-](https://doi.org/10.1038/s41561-018-0227-0)  
928 0227-0.
- 929 Geden, O., and A. Löschel, 2017: Define limits for temperature overshoot targets. *Nat. Geosci.*, **10**,  
930 881–882, <https://doi.org/10.1038/s41561-017-0026-z>.
- 931 Gillett, N. P., V. K. Arora, D. Matthews, and M. R. Allen, 2013: Constraining the Ratio of Global  
932 Warming to Cumulative CO<sub>2</sub> Emissions Using CMIP5 Simulations. *J. Clim.*, **26**, 6844–6858,  
933 <https://doi.org/10.1175/JCLI-D-12-00476.1>.
- 934 Goodwin, P., A. Katavouta, V. M. Roussenov, G. L. Foster, E. J. Rohling, and R. G. Williams, 2018:  
935 Pathways to 1.5 °C and 2 °C warming based on observational and geological constraints. *Nat.*  
936 *Geosci.*, **11**, 102–107, <https://doi.org/10.1038/s41561-017-0054-8>.
- 937 Gregory, J. M., C. D. Jones, P. Cadule, and P. Friedlingstein, 2009: Quantifying Carbon Cycle  
938 Feedbacks. *J. Clim.*, **22**, 5232–5250, <https://doi.org/10.1175/2009JCLI2949.1>.
- 939 Hajima, T., and Coauthors, 2020: Development of the MIROC-ES2L Earth system model and the  
940 evaluation of biogeochemical processes and feedbacks. *Geosci. Model Dev.*, **13**, 2197–2244,  
941 <https://doi.org/10.5194/gmd-13-2197-2020>.
- 942 Hugelius, G., and Coauthors, 2014: Estimated stocks of circumpolar permafrost carbon with quantified  
943 uncertainty ranges and identified data gaps. *Biogeosciences*, **11**, 6573–6593,  
944 <https://doi.org/10.5194/bg-11-6573-2014>.
- 945 Jeltsch-Thömmes, A., T. F. Stocker, and F. Joos, 2020: Hysteresis of the Earth system under positive  
946 and negative CO<sub>2</sub> emissions. *Environ. Res. Lett.*, **15**,  
947 124026, <https://doi.org/10.1088/1748-9326/abc4af>.
- 948 Jenkins, M., and A. Dai, 2021: The Impact of Sea-Ice Loss on Arctic Climate Feedbacks and Their  
949 Role for Arctic Amplification. *Geophys. Res. Lett.*, **48**, <https://doi.org/10.1029/2021GL094599>.
- 950 Jones, C. D., and Coauthors, 2016a: Simulating the Earth system response to negative emissions.  
951 *Environ. Res. Lett.*, **11**, 095012, <https://doi.org/10.1088/1748-9326/11/9/095012>.
- 952 Jones, C. D., and Coauthors, 2016b: C4MIP – The Coupled Climate–Carbon Cycle Model  
953 Intercomparison Project: experimental protocol for CMIP6. *Geosci. Model Dev.*, **9**, 2853–2880,  
954 <https://doi.org/10.5194/gmd-9-2853-2016>.
- 955 Keller, D. P., and Coauthors, 2018: The Carbon Dioxide Removal Model Intercomparison Project  
956 (CDRMIP): rationale and experimental protocol for CMIP6. *Geosci. Model Dev.*, **11**, 1133–  
957 1160, <https://doi.org/10.5194/gmd-11-1133-2018>.
- 958 Lawrence, D. M., and Coauthors, 2019: The Community Land Model Version 5: Description of New  
959 Features, Benchmarking, and Impact of Forcing Uncertainty. *J. Adv. Model. Earth Syst.*, **11**,  
960 4245–4287, <https://doi.org/10.1029/2018MS001583>.
- 961 Lenton, T. M., J. Rockström, O. Gaffney, S. Rahmstorf, K. Richardson, W. Steffen, and H. J.  
962 Schellnhuber, 2019: Climate tipping points — too risky to bet against. *Nature*, **575**, 592–595,



- 963 <https://doi.org/10.1038/d41586-019-03595-0>.
- 964 Li, X., K. Zickfeld, S. Mathesius, K. Kohfeld, and J. B. R. Matthews, 2020: Irreversibility of Marine  
965 Climate Change Impacts Under Carbon Dioxide Removal. *Geophys. Res. Lett.*, **47**,  
966 e2020GL088507, <https://doi.org/10.1029/2020GL088507>.
- 967 Liang, Y.-C., L. M. Polvani, and I. Mitevski, 2022: Arctic amplification, and its seasonal migration,  
968 over a wide range of abrupt CO<sub>2</sub> forcing. *Npj Clim. Atmospheric Sci.*, **5**, 14,  
969 <https://doi.org/10.1038/s41612-022-00228-8>.
- 970 Liddicoat, S. K., and Coauthors, 2021: Compatible Fossil Fuel CO<sub>2</sub> Emissions in the CMIP6 Earth  
971 System Models' Historical and Shared Socioeconomic Pathway Experiments of the Twenty-  
972 First Century. *J. Clim.*, **34**, 2853–2875, <https://doi.org/10.1175/JCLI-D-19-0991.1>.
- 973 MacDougall, A. H., K. Zickfeld, R. Knutti, and H. D. Matthews, 2015: Sensitivity of carbon budgets to  
974 permafrost carbon feedbacks and non-CO<sub>2</sub> forcings. *Environ. Res. Lett.*, **10**, 125003,  
975 <https://doi.org/10.1088/1748-9326/10/12/125003>.
- 976 Mathesius, S., M. Hofmann, K. Caldeira, and H. J. Schellnhuber, 2015: Long-term response of oceans  
977 to CO<sub>2</sub> removal from the atmosphere. *Nat. Clim. Change*, **5**, 1107–1113,  
978 <https://doi.org/10.1038/nclimate2729>.
- 979 Meehl, G. A., C. A. Senior, V. Eyring, G. Flato, J.-F. Lamarque, R. J. Stouffer, K. E. Taylor, and M.  
980 Schlund, 2020: Context for interpreting equilibrium climate sensitivity and transient climate  
981 response from the CMIP6 Earth system models. *Sci. Adv.*, **6**, eaba1981,  
982 <https://doi.org/10.1126/sciadv.aba1981>.
- 983 Melnikova, I., and Coauthors, 2021: Carbon Cycle Response to Temperature Overshoot Beyond 2°C:  
984 An Analysis of CMIP6 Models. *Earths Future*, **9**, e2020EF001967,  
985 <https://doi.org/10.1029/2020EF001967>.
- 986 Melnikova, I., and Coauthors, 2022: Impact of bioenergy crop expansion on climate–carbon cycle  
987 feedbacks in overshoot scenarios. *Earth Syst. Dyn.*, **13**, 779–794, <https://doi.org/10.5194/esd-13-779-2022>.
- 989 O'Neill, B. C., E. Kriegler, K. Riahi, K. L. Ebi, S. Hallegatte, T. R. Carter, R. Mathur, and D. P. van  
990 Vuuren, 2014: A new scenario framework for climate change research: the concept of shared  
991 socioeconomic pathways. *Clim. Change*, **122**, 387–400, <https://doi.org/10.1007/s10584-013-0905-2>.
- 993 O'Neill, B. C., and Coauthors, 2016: The Scenario Model Intercomparison Project (ScenarioMIP) for  
994 CMIP6. *Geosci. Model Dev.*, **9**, 3461–3482, <https://doi.org/10.5194/gmd-9-3461-2016>.
- 995 Park, S.-W., and J.-S. Kug, 2022: A decline in atmospheric CO<sub>2</sub> levels under negative emissions may  
996 enhance carbon retention in the terrestrial biosphere. *Commun. Earth Environ.*, **3**, 1–8,  
997 <https://doi.org/10.1038/s43247-022-00621-4>.
- 998 Riahi, K., and Coauthors, 2021: Cost and attainability of meeting stringent climate targets without  
999 overshoot. *Nat. Clim. Change*, **11**, 1063–1069, <https://doi.org/10.1038/s41558-021-01215-2>.
- 1000 Ricke, K. L., R. J. Millar, and D. G. MacMartin, 2017: Constraints on global temperature target  
1001 overshoot. *Sci. Rep.*, **7**, 14743, <https://doi.org/10.1038/s41598-017-14503-9>.
- 1002 Rogelj, J., M. Meinshausen, M. Schaeffer, R. Knutti, and K. Riahi, 2015: Impact of short-lived non-CO  
1003  $\text{less}\text{sub}\text{greater}\text{2}\text{less}\text{/sub}\text{greater}\text{\$}$  mitigation on carbon budgets for stabilizing global  
1004 warming. *Environ. Res. Lett.*, **10**, 075001, <https://doi.org/10.1088/1748-9326/10/7/075001>.
- 1005 Roy, T., and Coauthors, 2011: Regional Impacts of Climate Change and Atmospheric CO<sub>2</sub> on Future  
1006 Ocean Carbon Uptake: A Multimodel Linear Feedback Analysis. *J. Clim.*, **24**, 2300–2318,  
1007 <https://doi.org/10.1175/2010JCLI3787.1>.
- 1008 —, J. B. Sallée, L. Bopp, and N. Metzl, 2021: Diagnosing CO<sub>2</sub>-Emission-Induced Feedbacks  
1009 between the Southern Ocean Carbon Cycle and the Climate System: A Multiple Earth System  
1010 Model Analysis Using a Water Mass Tracking Approach. *J. Clim.*, **34**, 9071–9092,  
1011 <https://doi.org/10.1175/JCLI-D-20-0889.1>.



- 1012 Schimel, D., B. B. Stephens, and J. B. Fisher, 2015: Effect of increasing CO<sub>2</sub> on the terrestrial carbon  
1013 cycle. *Proc. Natl. Acad. Sci.*, **112**, 436–441, <https://doi.org/10.1073/pnas.1407302112>.
- 1014 Schuur, E. A. G., and Coauthors, 2015: Climate change and the permafrost carbon feedback. *Nature*,  
1015 **520**, 171–179, <https://doi.org/10.1038/nature14338>.
- 1016 Schwinger, J., and J. Tjiputra, 2018: Ocean Carbon Cycle Feedbacks Under Negative Emissions.  
1017 *Geophys. Res. Lett.*, **45**, 5062–5070, <https://doi.org/10.1029/2018GL077790>.
- 1018 —, and Coauthors, 2014: Nonlinearity of Ocean Carbon Cycle Feedbacks in CMIP5 Earth System  
1019 Models. *J. Clim.*, **27**, 3869–3888, <https://doi.org/10.1175/JCLI-D-13-00452.1>.
- 1020 —, A. Asaadi, N. J. Steinert, and H. Lee, 2022: Emit now, mitigate later? Earth system reversibility  
1021 under overshoots of different magnitudes and durations. *Earth Syst. Dyn.*, **13**, 1641–1665,  
1022 <https://doi.org/10.5194/esd-13-1641-2022>.
- 1023 Séférian, R., and Coauthors, 2019: Evaluation of CNRM Earth System Model, CNRM-ESM2-1: Role  
1024 of Earth System Processes in Present-Day and Future Climate. *J. Adv. Model. Earth Syst.*, **11**,  
1025 4182–4227, <https://doi.org/10.1029/2019MS001791>.
- 1026 Seland, Ø., and Coauthors, 2020: Overview of the Norwegian Earth System Model (NorESM2) and  
1027 key climate response of CMIP6 DECK, historical, and scenario simulations. *Geosci. Model  
1028 Dev.*, **13**, 6165–6200, <https://doi.org/10.5194/gmd-13-6165-2020>.
- 1029 Sellar, A. A., and Coauthors, 2019: UKESM1: Description and Evaluation of the U.K. Earth System  
1030 Model. *J. Adv. Model. Earth Syst.*, **11**, 4513–4558, <https://doi.org/10.1029/2019MS001739>.
- 1031 Smith, S. L., H. B. O’Neill, K. Isaksen, J. Noetzli, and V. E. Romanovsky, 2022: The changing thermal  
1032 state of permafrost. *Nat. Rev. Earth Environ.*, **3**, 10–23, <https://doi.org/10.1038/s43017-021-00240-1>.
- 1033
- 1034 Swart, N. C., and Coauthors, 2019: The Canadian Earth System Model version 5 (CanESM5.0.3).  
1035 *Geosci. Model Dev.*, **12**, 4823–4873, <https://doi.org/10.5194/gmd-12-4823-2019>.
- 1036 Taylor, K. E., R. J. Stouffer, and G. A. Meehl, 2012: An Overview of CMIP5 and the Experiment  
1037 Design. *Bull. Am. Meteorol. Soc.*, **93**, 485–498, <https://doi.org/10.1175/BAMS-D-11-00094.1>.
- 1038 Tharammal, T., G. Bala, N. Devaraju, and R. Nemani, 2019: A review of the major drivers of the  
1039 terrestrial carbon uptake: model-based assessments, consensus, and uncertainties. *Environ. Res.  
1040 Lett.*, **14**, 093005, <https://doi.org/10.1088/1748-9326/ab3012>.
- 1041 Tjiputra, J. F., and Coauthors, 2020: Ocean biogeochemistry in the Norwegian Earth System Model  
1042 version 2 (NorESM2). *Geosci. Model Dev.*, **13**, 2393–2431, <https://doi.org/10.5194/gmd-13-2393-2020>.
- 1043
- 1044 Tokarska, K. B., and K. Zickfeld, 2015: The effectiveness of net negative carbon dioxide emissions in  
1045 reversing anthropogenic climate change. *Environ. Res. Lett.*, **10**, 094013,  
1046 <https://doi.org/10.1088/1748-9326/10/9/094013>.
- 1047 V. Masson-Delmotte, P. Zhai, H.-O. Pörtner, D. Roberts, J. Skea, P.R. Shukla, A. Pirani, and W.  
1048 Moufouma-Okia, C. Péan, R. Pidcock, S. Connors, J.B.R. Matthews, Y. Chen, X. Zhou, M.I.  
1049 Gomis, E. Lonnoy, T. Maycock, M. Tignor, and T. Waterfield, 2018: IPCC, 2018: Summary for  
1050 Policymakers. In: Global Warming of 1.5°C. An IPCC Special Report on the impacts of global  
1051 warming of 1.5°C above pre-industrial levels and related global greenhouse gas emission  
1052 pathways, in the context of strengthening the global response to the threat of climate change,  
1053 sustainable development, and efforts to eradicate poverty, 32 pp. <https://www.ipcc.ch/sr15/>  
1054 (Accessed June 21, 2021).
- 1055 de Vrese, P., and V. Brovkin, 2021: Timescales of the permafrost carbon cycle and legacy effects of  
1056 temperature overshoot scenarios. *Nat. Commun.*, **12**, 2688, <https://doi.org/10.1038/s41467-021-23010-5>.
- 1057
- 1058 Wu, P., J. Ridley, A. Pardaens, R. Levine, and J. Lowe, 2015: The reversibility of CO<sub>2</sub> induced climate  
1059 change. *Clim. Dyn.*, **45**, 745–754, <https://doi.org/10.1007/s00382-014-2302-6>.
- 1060 Yang, S., D. Tian, J. Chou, T. Wei, X. Zhu, and W. Dong, 2021: Reversibility of historical and future



!061 climate change with a complex earth system model. *Theor. Appl. Climatol.*, **146**, 1061–1068,  
!062 <https://doi.org/10.1007/s00704-021-03757-z>.  
!063 Yokohata, T., K. Saito, A. Ito, H. Ohno, K. Tanaka, T. Hajima, and G. Iwahana, 2020: Future  
!064 projection of greenhouse gas emissions due to permafrost degradation using a simple numerical  
!065 scheme with a global land surface model. *Prog. Earth Planet. Sci.*, **7**, 56,  
!066 <https://doi.org/10.1186/s40645-020-00366-8>.  
!067 Yoshikawa, C., M. Kawamiya, T. Kato, Y. Yamanaka, and T. Matsuno, 2008: Geographical  
!068 distribution of the feedback between future climate change and the carbon cycle. *J. Geophys.*  
!069 *Res. Biogeosciences*, **113**, <https://doi.org/10.1029/2007JG000570>.  
!070  
!071  
!072  
!073  
!074  
!075